

1 **Nomograms of Human Hippocampal Volume** 2 **Shifted by Polygenic Scores**

3 Mohammed Janahi^{1,2}, Leon Aksman³, Jonathan M Schott⁴, Younes Mokrab^{2,5} and
4 Andre Altmann¹ for the Alzheimer's Disease Neuroimaging Initiative *

5 1 Centre for Medical Image Computing (CMIC), Department of Medical Physics and Biomedical Engineering, University College
6 London, United Kingdom

7 2 Medical and Population Genomics Lab, Human Genetics Department, Research Branch, Sidra Medicine, Doha, Qatar

8 3 Stevens Neuroimaging and Informatics Institute, Keck School of Medicine, University of Southern California, Los Angeles, CA, United
9 States of America

10 4 Dementia Research Centre (DRC), Queen Square Institute of Neurology, University College London, United Kingdom

11 5 Department of Genetic Medicine, Weill Cornell Medicine-Qatar, Doha, Qatar

12 * Data used in the preparation of this article were obtained from the Alzheimer's Disease Neuroimaging Initiative (ADNI) database
13 (adni.loni.usc.edu). As such, the investigators within the ADNI contributed to the design and implementation of ADNI and/or provided
14 data but did not participate in analysis or writing of this report. A complete listing of ADNI investigators can be found at:
15 http://adni.loni.usc.edu/wp-content/uploads/how_to_apply/ADNI_Acknowledgement_List.pdf.

16
17
18
19
20
21
22
23
24
25
26
27
28
29
30
31
32
33
34
35
36

37 **Abstract**

38

39 Nomograms are important clinical tools applied widely in both developing and aging
40 populations. They are generally constructed as normative models identifying cases as
41 outliers to a distribution of healthy controls. Currently used normative models do not
42 account for genetic heterogeneity. Hippocampal Volume (HV) is a key endophenotype for
43 many brain disorders. Here, we examine the impact of genetic adjustment on HV
44 nomograms and the translational ability to detect dementia patients. Using imaging data
45 from 35,686 healthy subjects aged 44 to 82 from the UK BioBank (UKB), we built HV
46 nomograms using gaussian process regression (GPR), which - compared to a previous
47 method - extended the application age by 20 years, including dementia critical age ranges.
48 Using HV Polygenic Scores (HV-PGS), we built genetically adjusted nomograms from
49 participants stratified into the top and bottom 30% of HV-PGS. This shifted the nomograms
50 in the expected directions by $\sim 100 \text{ mm}^3$ (2.3% of the average HV), which equates to 3 years
51 of normal aging for a person aged ~ 65 . Clinical impact of genetically adjusted nomograms
52 was investigated by comparing 818 subjects from the AD neuroimaging (ADNI) database
53 diagnosed as either cognitively normal (CN), having mild cognitive impairment (MCI) or
54 Alzheimer's disease patients (AD). While no significant change in the survival analysis was
55 found for MCI-to-AD conversion, an average of 68% relative decrease was found in intra-
56 diagnostic-group variance, highlighting the importance of genetic adjustment in untangling
57 phenotypic heterogeneity.

58

59

60

61

62

63

64

65

66

67

68

69

70

71

72

73

74 **Introduction**

75

76 Brain imaging genetics is a rapidly evolving area of neuroscience combining imaging,
77 genetic, and clinical data to gain insight into normal and diseased brain morphology and
78 function¹. Normative modelling is an emerging method in neuroscience, aiming to identify
79 cases as outliers to a distribution of healthy controls and was shown to have potential to
80 improve early diagnosis, progression models, and risk assessment²⁻⁵. Where conventional
81 case-control studies generally require both cases and controls to be well clustered,
82 normative models work well even when cases are not clustered or overlap with controls.
83 Nomograms are a common implementation of normative models and have been used as
84 growth charts of brain volumes across age in both developing and aging populations⁶⁻⁸.

85

86 Normative modelling identifies cases by their deviation from normality, however, genetics
87 shapes what is 'normal'. Heritability studies have found that whole brain volume is
88 $90\% \pm 4.8\%$ heritable⁹, hippocampal volume is $75\% \pm 5\%$ ¹⁰⁻¹², and other cortical brain
89 areas between 34% and 80%^{13,14}. Genome-wide association studies (GWAS) have identified
90 genome wide significant variants that explain $13\% \pm 1.5\%$ of the variation in hippocampal
91 volume (HV)¹⁵, $34\% \pm 3\%$ in total cortical surface area, and $26\% \pm 2\%$ in average cortical
92 thickness¹⁶. The gap between estimates from GWAS hits and formal heritability estimates
93 (termed the 'missing heritability')¹⁷ implies that less significant variants also have an
94 influence and that it may be captured through polygenic scores (PGS)¹⁸⁻²⁰. In this work we
95 demonstrate the impact of accounting for polygenic effects in normative modelling of HV.

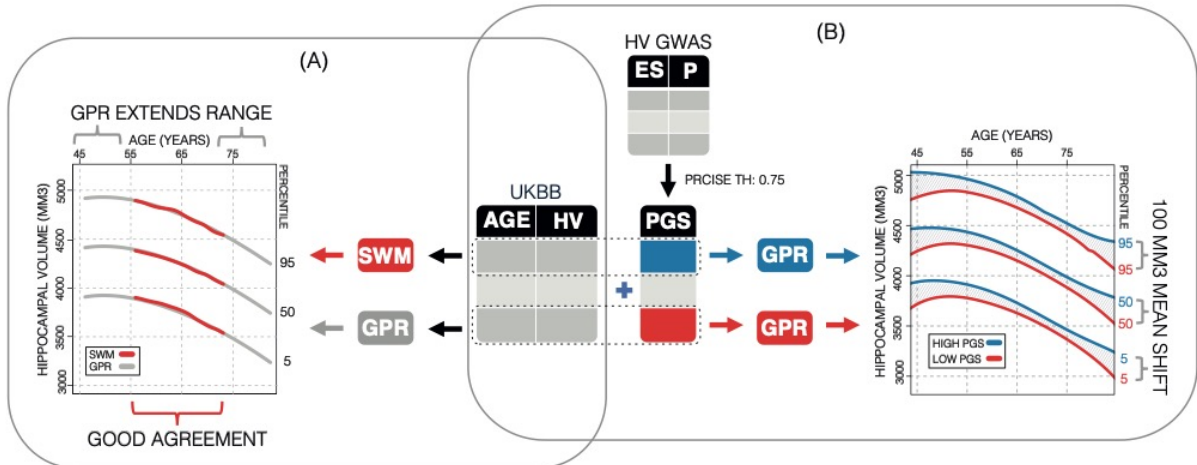
96

97 Damage to the hippocampus (which is integral to memory processes²¹) has been associated
98 with major depressive disorder²², schizophrenia²³, Epilepsy²⁴, and Alzheimer's disease
99 (AD)²⁵. AD is a global health burden: 7% percent of people over 60 are diagnosed with
100 dementia²⁶ of which AD accounts for 70%²⁷. The pathophysiological processes underlying
101 AD, namely amyloid and tau pathology accumulation, are thought to precede brain atrophy,
102 which typically starts in the hippocampus and medial temporal lobe and then spreads
103 throughout the neocortex²⁷.

104

105 The normal variation of HV is of great clinical interest as the early and often prominent
106 hippocampal atrophy seen in AD creates a need for early diagnosis and disease tracking.

107 Many studies have examined HV across age^{28,29}, for example, a recent study by Nobis et.
108 (2019)³⁰ produced HV nomograms from UK Biobank (UKB) for use in clinical settings. It is
109 important to note that some of the variation in the normative models can be explained by
110 the clear impact of genetics on HV^{15,31}. Thus far, the few attempts at including genetics in
111 the construction of HV nomograms have focussed on disease related variants. For instance,
112 two recent studies examined the impact of the AD-associated *APOE* gene^{32,33}, showing that
113 *APOE4/4* carriers had significantly lower HV trajectories. This effect is likely driven by AD-
114 related disease processes since *APOE4/4* carriers have a 10-fold risk of developing AD^{34,35}.
115 However, the genetic impact on variation in HV in healthy population remains
116 underexamined in the context of nomograms. In this work, we close this gap. We built HV
117 nomograms using a gaussian process regression (GPR) method (Figure 1A). We then
118 computed a PGS of HV for subjects in our cohort and built genetically adjusted nomograms
119 (Figure 1B). We found that genetic adjustment did in fact shift the nomograms and that,
120 because the model requires no smoothing, our GPR nomograms provided an extended age
121 range compared to previous methods.



122

123 **Figure 1: Study Overview.** (A) Using 35,686 subjects from the UK BioBank, we generate
 124 nomograms using two methods: a previously reported Sliding Window Method (SWM), and
 125 Gaussian Process Regression (GPR). We find that GPR is more data efficient than the SWM
 126 and can extend the nomogram into dementia critical age ranges. (B) Using a previously
 127 reported genome wide association study, we generate polygenic scores (PGS) for the
 128 subjects in our UK BioBank table. We then stratify the table by PGS and generate
 129 nomograms for the top and bottom 30% of samples separately. We find the genetic
 130 adjustment differentiates the nomograms by an average of 100 mm³, which is equivalent to
 131 about 3 years of normal aging for a 65-year-old.

132

133

134

135

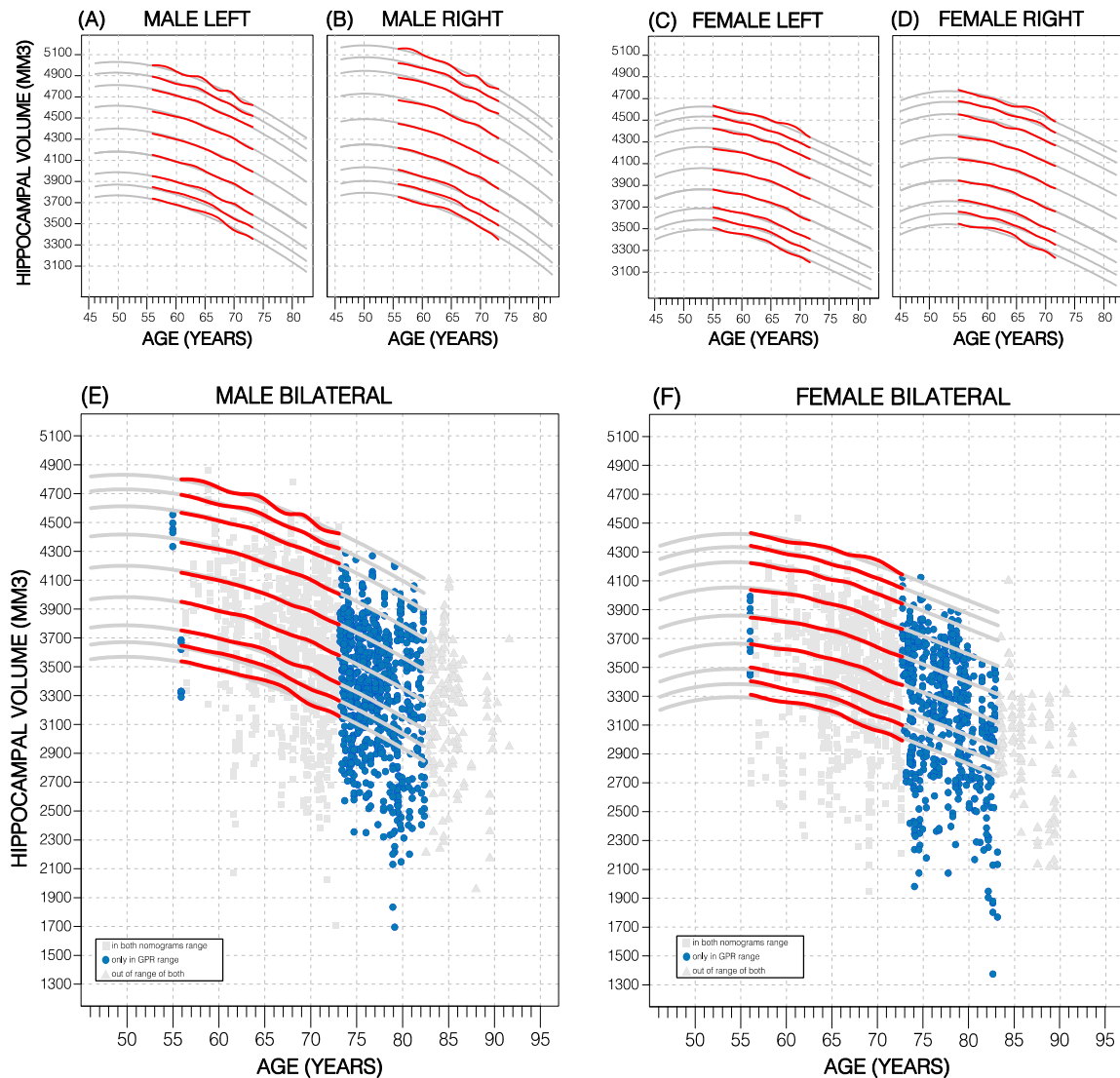
136 **Results**

137 In the UKB sample 453 subjects were excluded for various conditions, 3497
138 for genetic ancestry, and 28 subjects were outliers: leaving a total of 35,686 subjects. In the
139 ADNI application dataset, 26 subjects were excluded for genetic ancestry, and 314 based on
140 HV quality scores: leaving 818 subjects.

141

142 *SWA vs GPR for nomogram estimation*

143 Nomograms of healthy subjects generated using the SWA and GPR method displayed similar
144 trends (Figure 2; Figure 2 – Figure Supplement 2). However, GPR nomograms spanned the
145 entire training dataset age range (45-82 years) compared to the SWA (52-72 years). This is
146 primarily because the SWA is a non-model-based approach that requires smoothing to avoid
147 edge effects, and a gaussian smoothing window of width 20 was used³⁰. This extension
148 allowed 86% of all diagnostic groups from the ADNI to be evaluated versus 56% in the SWA
149 Nomograms (Figure 2; Figure 2 – Figure Supplement 2). Furthermore, our GPR nomograms
150 confirmed previously reported trends: Overall, the average 50th percentile in male
151 nomograms (4162 ± 222) was higher than the female nomograms (3883 ± 170), and
152 within each sex, right HV was larger than left HV (Figure 2; Figure 2 – Figure Supplement 2).
153 We also observed that along the 50th percentile, male HV declined faster ($-20.3 \text{ mm}^3/\text{year}$)
154 than female HV ($-14.6 \text{ mm}^3/\text{year}$). Additionally, in GPR nomograms, HV peaks in women at
155 age 53.5 years with a less pronounced peak in males at 50 years (Figure 2; Figure 2 – Figure
156 Supplement 2). Training the GRP model with 16,000 samples took ~1 hour on a consumer
157 grade machine (2.3 GHz 8-Core Intel Core i9).



158

159 **Figure 2: Comparing Nomogram Generation Methods.** Nomograms produced from healthy
 160 UKB subjects using the sliding window approach (SWA) (red lines) and gaussian process
 161 regression (GPR) method (grey lines) show similar trends. both left hemisphere nomograms
 162 (A, C) are lower than their right counterparts (B, D). Male nomograms are higher than
 163 female nomograms (A vs C) and (B vs D). Female HV shows a peak at 53.5 years of age, while
 164 male HV shows a less prominent peak at 50 years of age. SWA and GPR show good
 165 agreement, while GPR enables a 10-year nomogram extension in either direction. The
 166 benefits of this extension can be seen with scatter plots of ADNI subjects of all diagnoses
 167 overlaid (E, F). The extended age range of the GPR nomograms (45-82 years) enables the
 168 evaluation of an additional 43% of male data (E) and 34% of female data (F) (turquoise
 169 circles). A similar figure with only the Cognitively Normal ADNI subjects can be found in
 170 Figure 2 – Figure Supplement 2

171

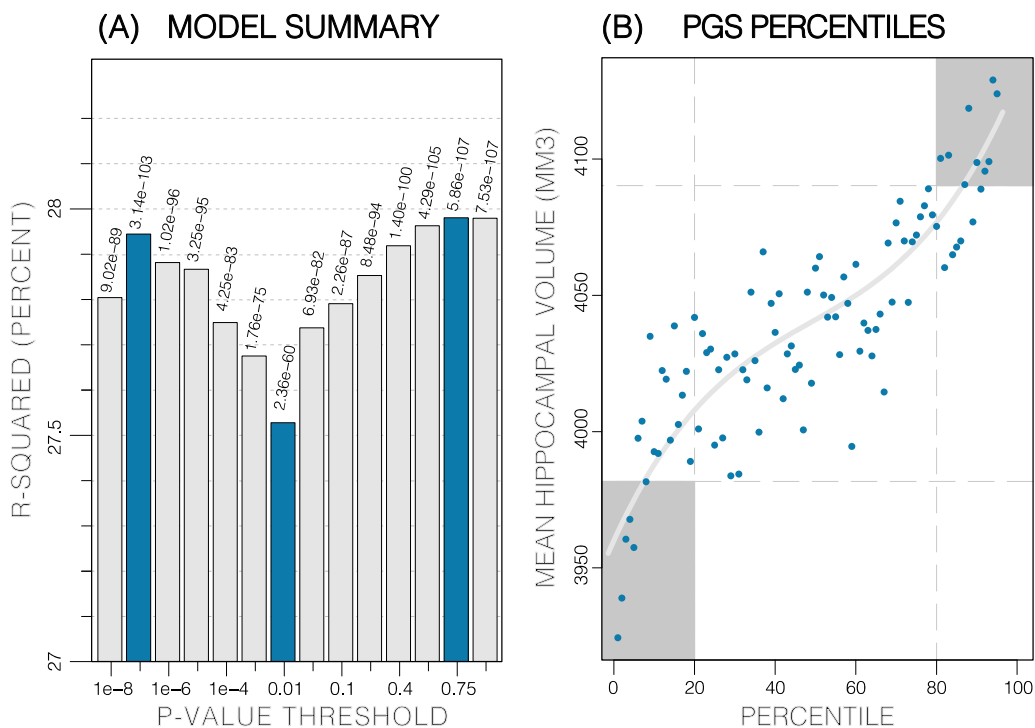
172

173

174 *Polygenic Score for Hippocampal Volume*

175 The calculated PGS, based on an earlier GWAS for average bilateral hippocampal volume¹⁵,
 176 as expected, showed a strong correlation with HV in the UKB data. Overall, the PGSs showed
 177 a significant positive correlation with HV across all p -value thresholds and training sample
 178 subsets ($p < 2.7 \times 10^{-24}$; Table 1). PGSs explained more variance in males versus females.
 179 Furthermore, PGSs did not show detectable differences in left versus right HV; and
 180 explained the most variance in mean bilateral HV (Table 1, Figure 3 – Data Source 1). In all
 181 tested settings, the explained variance (R^2) by the PGS across p -value threshold was similar:
 182 with one peak at the 1×10^{-7} threshold (capturing few but very significant SNPs), a higher peak
 183 at the 0.75 threshold (capturing many SNPs with mostly small effect sizes) (Figure 3). For the
 184 ADNI dataset, this distribution increased with the threshold. When investigating mean HV
 185 across percentile of PGS at the 0.75 threshold (highest R^2), the top and bottom 20% of
 186 scores accounted for 41% of the variance in HV (Figure 3); with similar values observed
 187 across thresholds in both datasets (Figure 3 – Figure Supplement 1, 2).

188



189
 190

191 **Figure 3: Summary of PGS models.** Polygenic Risk Score in models of mean HV across both
 192 sexes. (a) R^2 of linear models across increasing p-value thresholds. All models are of bilateral
 193 HV and account for age, sex, and top 10 genetic principal components. The minimum R^2 on

194 the y-scale is the R^2 of the models without any PGS. (b) distribution of mean HV across
 195 percentiles of PGS. Excluding the top and bottom 20% of percentiles reduces the variance by
 196 49% (darker grey areas). Fitting a cubic polynomial to the means produces the grey line.
 197

198 **Table 1: Association between Polygenic Scores (PGS) and Hippocampal Volume (HV).**

199 Linear models were built for HV (left; right; bilateral) using PGS across cohorts (male;
 200 female; both) at three representative p -value thresholds (1E-7; 0.01; 1). p -values of the
 201 slope were significant across all categories, with the lowest being associated with the
 202 threshold value of 1 in all but a single case (both/right). Variance explained (R^2) increased
 203 from left to right to bilateral volumes and increased from female to male to both.
 204

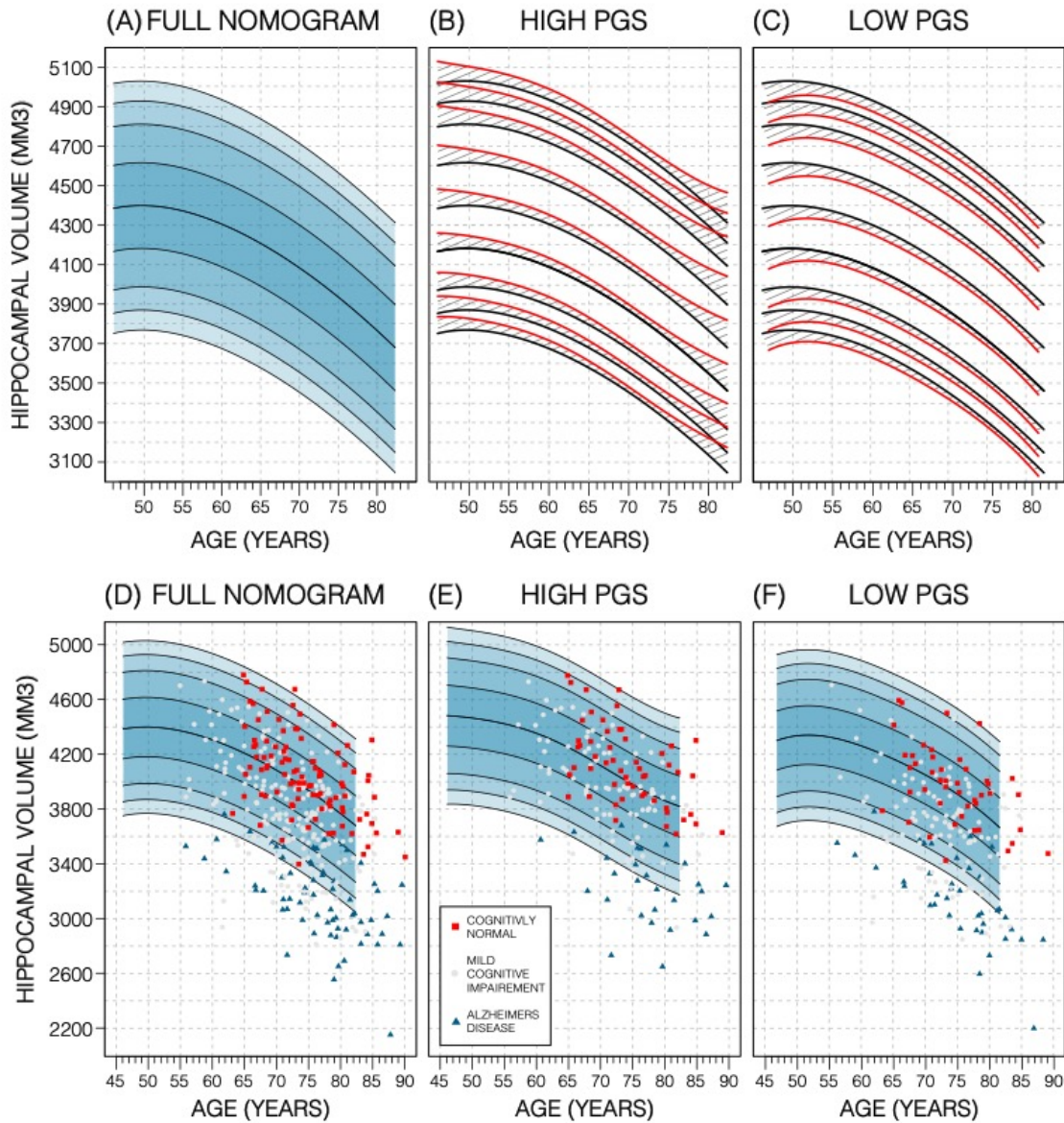
Gender	PGS threshold	LEFT			RIGHT			BILATERAL		
		Slope ($\times 10^{-2}$)	p -value	R^2	Slope ($\times 10^{-2}$)	p -value	R^2	Slope ($\times 10^{-2}$)	p -value	R^2
FEMALE	1E-7	10	1.8E-46	13%	9.4	2.4E-45	14%	11	1.4E-51	15%
	0.01	8.2	2.7E-26	13%	7.6	1.0E-27	13%	8.7	3.2E-30	14%
	1	11	9.4E-54	13%	9.62	1.5E-48	14%	11	1.6E-57	15%
MALE	1E-7	8.2	1.4E-35	18%	7.5	2.6E-35	18%	9.2	4.1E-40	20%
	0.01	7.8	3.8E-29	18%	6.8	3.8E-27	18%	8.6	7.8E-32	20%
	1	9.4	3.2E-48	18%	8.0	4.7E-43	18%	10	9.1E-52	20%
BOTH	1E-7	8.4	8.1E-90	25%	7.9	6.4E-93	26%	9.3	3.1E-103	28%
	0.01	7.4	9.3E-54	24%	6.7	3.3E-53	26%	8	2.3E-60	28%
	1	9.6	2.1E-99	25%	8.3	1.8E-89	26%	10	7.5E-107	28%

205
 206 Slope = beta coefficient for PGS in the linear mode; p -value for the slope; R^2 = variance
 207 explained by the linear model
 208

209 *Genetics stratified Nomograms*

210
 211 We will focus on the p -value threshold of 0.75 as it achieved best or close to-best
 212 performance overall (Figure 3 – Data Source 1). Genetics had a clear effect on the
 213 nomograms: the high-PGS nomograms were shifted upwards while the low-PGS nomograms
 214 were shifted downwards; an effect which could be observed at both the model and data
 215 level (Figure 4; Figure 4 – Figure Supplement 3), both by around 1.2% of the average HV (50
 216 mm^3). Thus, the difference between high and low PGS nomograms was $\sim 2.3\%$ of the
 217 average HV (100 mm^3). An ANOVA test of the percentiles produced with the adjusted vs
 218 unadjusted nomograms revealed that the groups were significantly different to each other
 219 ($F > 19$; $P < 8.04 \times 10^{-6}$; Table 2). The HV peak previously observed at 50 years in males was less
 220 pronounced in the high-PGS nomogram and more so in the low-PGS nomogram (Figure 4,
 221 Figure 4 – Figure Supplement 1). Adjusting nomograms using ICV and AD PGSs, instead of

222 HV PGS, did not result in nomograms that were meaningfully different from the non-
 223 adjusted nomograms (Figure 4 – Figure Supplement 2).



224
 225 **Figure 4: Genetically Adjusted Nomograms.** Results of genetic adjustment in bilateral male
 226 hippocampal volume (HV). (A, D) Nomograms of bilateral hippocampal volume (HV)
 227 generated from all male UKB samples overlaid with male ADNI samples. CN samples (red
 228 squares) centre around the 50th percentile, AD samples (turquoise triangles) lie mostly
 229 below the 2.5th percentile, and MCI samples (grey circles) span both regions. (B, E)
 230 Nomograms generated using only high PGS samples (top 30%) was shifted upward (red
 231 lines) compared to the original (black lines) by an average of 50 mm³ (1.2% of mean HV).
 232 Plotting the high PGS ADNI samples (top 50%) slightly improves intra-group variance. (C, F)
 233 similar results are seen in low PGS samples. Note, the black lines in panels (B, C) are the
 234 same as the nomogram in panel (A) and similarly the red lines in panel (B, C) are same as the
 235 nomogram in panels (E, F).
 236

237 **Table 2: Results of ANOVA tests of UKB HV Percentiles produced with genetically adjusted**
 238 **and unadjusted nomograms.**

SEX	STRATA	DF	SUM SQ	F-VALUE	P-VALUE
MEN	HIGH	1	18786	22.84	1.8e-06 ***
	LOW	1	16407	19.96	8.04e-06 ***
WOMEN	HIGH	1	27068	32.92	9.97e-09 ***
	LOW	1	30103	36.94	1.28e-09 ***

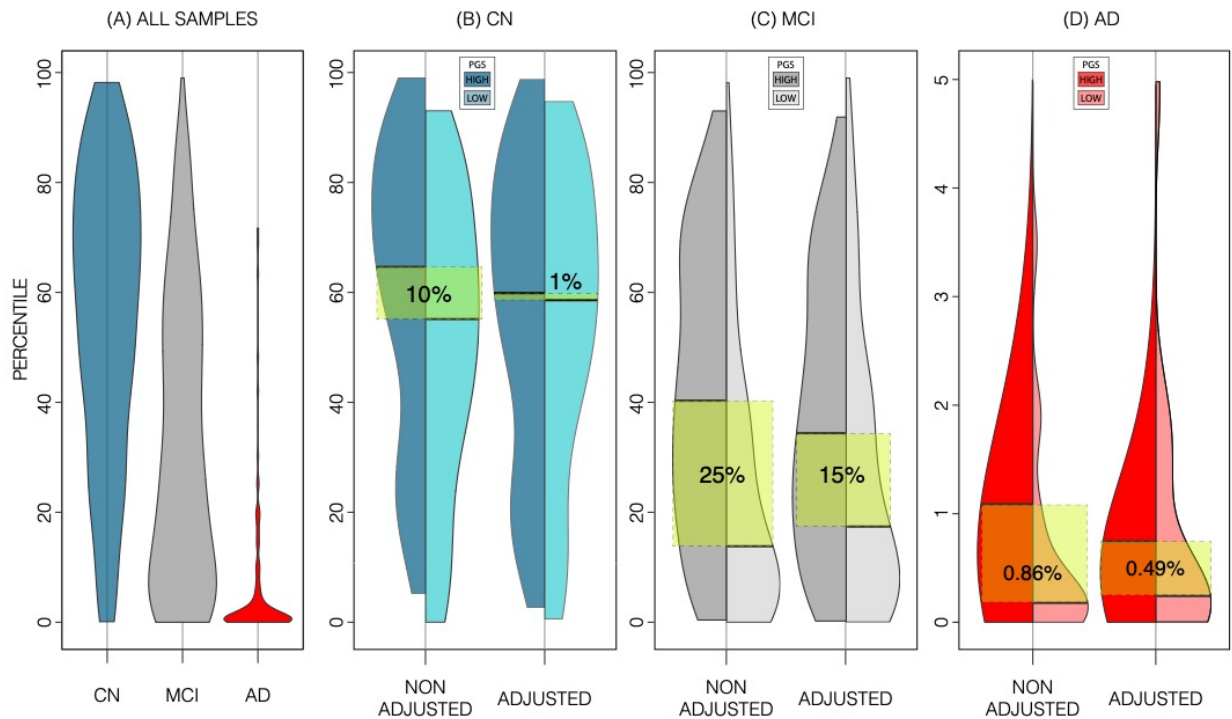
239

240

241 *External Evaluation on ADNI data*

242 In the ADNI dataset we investigated whether the shift in genetically adjusted nomograms
 243 could be leveraged for improved diagnosis. Using the non-adjusted nomogram, cognitively
 244 normal (CN) participants ($n = 225$) had a median bilateral HV percentile of 61% ($\pm 25\%$ SD),
 245 Mild Cognitive Impairment (MCI) participants ($n = 391$) had 25% ($\pm 26\%$ SD), and Alzheimer’s
 246 Disease (AD) participants ($n = 121$) had 1% ($\pm 9\%$ SD) (Figure 5). Visual inspection revealed
 247 that while CN participants were spread across the quantiles, AD participants lay mostly
 248 below the 2.5% quantile, and MCI participants spanned the range of both CN and AD
 249 participants (Figure 4). Bisecting the samples by PGS showed that high PGS CN samples had
 250 median percentiles of 65% ($\pm 27\%$ SD) and low PGS had 54% ($\pm 26\%$ SD). When comparing the
 251 same samples against the genetically adjusted nomograms instead, high PGS CN samples
 252 had 60% ($\pm 26\%$ SD) and low PGS had 59% ($\pm 26\%$ SD). Thus, reducing the gap between high
 253 and low PGS CN participants by 9% (from 10% to 1%; a 90% relative reduction). Similar
 254 analysis showed a reduction in MCI participants by 10% (60% relative reduction), and 0.5%
 255 (56% relative reduction) in AD participants. The above effects persisted across most strata
 256 (i.e., sex and hemisphere) (Figure 5; Figure 5 – Data Source 1).

257



258

259

Figure 5: ADNI Dataset Percentiles in Genetically Adjusted/Non-Adjusted Nomograms.

260

Plotting the percentile distribution of the different diagnostic groups across adjusted and

261

non-adjusted nomograms reveals that genetic adjustment increases group cohesiveness. (A)

262

The percentile distributions of the different diagnostic groups against the non-adjusted

263

nomograms. (B) In CN samples for example, when plotting against the non-adjusted

264

nomogram (left adjoined boxplots), the median percentile of the top 30% of samples

265

(darker turquoise) was 65%, while the median for the lower 30% of samples (lighter

266

turquoise) was 54%. When using the genetically adjusted nomogram instead (right adjoined

267

boxplots), those median percentiles become 60% and 59% respectively; a 90% relative

268

reduction. Similar results can be seen with MCI (C) and AD (D) samples, with 60% and 56%

269

relative reduction respectively.

270

271

Longitudinal Evaluation

272

We also investigated whether genetically adjusted nomograms provided additional accuracy

273

in distinguishing stable ($n = 299$) from MCI-to-AD progressing subjects ($n = 83$). With the

274

non-adjusted nomogram, progressing MCI participants had a mean HV percentile of 11%

275

and stable participants had 29% (Figure 6). Using the genetically adjusted nomograms, they

276

had 10% and 28%, respectively. Cox proportional hazards models of percentiles obtained

277

using both nomograms revealed little difference between the two in terms of clinical

278

conversion: both models resulted in a hazard ratio of 0.97 for percentile in nomogram (beta

279

of -0.03 at p -value $< 4.87e-08$); confirming that participants within lower HV percentiles

280

where more likely to convert earlier.

281
 282
 283
 284
 285
 286
 287
 288
 289
 290
 291
 292
 293
 294
 295
 296
 297
 298
 299
 300
 301
 302
 303
 304
 305
 306
 307
 308
 309
 310
 311
 312
 313
 314
 315

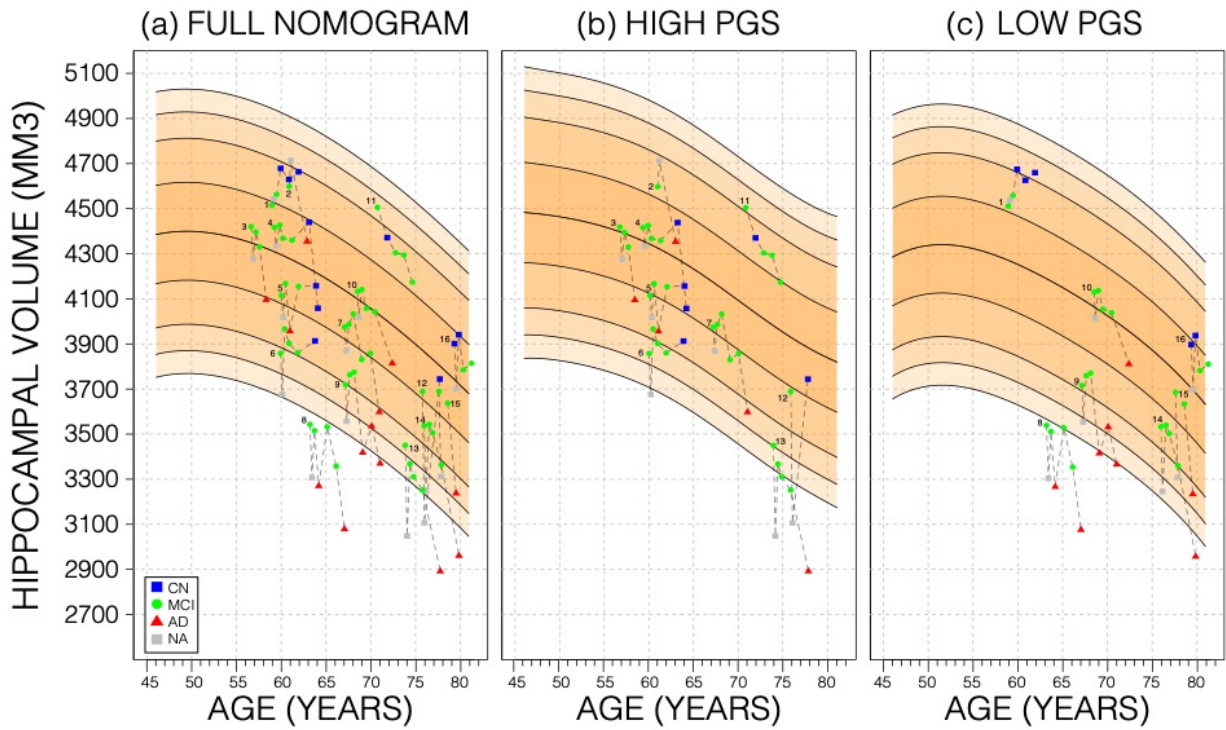


Figure 6: Longitudinal Analysis. A selection of MCI samples longitudinal data plotted against nomograms of male mean HV. (a) all selected samples plotted against a non-adjusted nomogram. Lines connect visits of the same sample with diagnosis at each visit shown: CN as blue squares; MCI as green dots, AD as red triangles, and no diagnosis (NA) as grey squares. (b) samples from (a) with high PGS plotted against a nomogram generated from high PGS CN samples in UKB. (c) equivalent result for low PGS samples from (a). For all sub-figures, the black lines -from top to bottom- represent the 2.5%, 5%, 10%, 25%, 50%, 75%, 90%, 95%, and 97.5% quantiles respectively.

316 **Discussion**

317

318 We hypothesized that inclusion of genetic information associated with regional brain
319 volume may substantially affect normative models. Indeed, the PGS for HV was significantly
320 positively correlated with estimated HV from MRI; translating into a shift of around 100
321 mm³ in nomograms based on PGS stratification (high vs low PGS). Importantly, this
322 magnitude corresponds to ~3 years' worth of HV loss during normal aging for a 65-year-old.
323 While previous studies have examined the impact of disease associated variants, such as
324 *APOE* status, on HV^{32,33} our study relied on genetic variants influencing HV in healthy
325 subjects. This is an important difference: the *APOE* genotype is associated with present or
326 future AD status rather than having a direct influence on HV in healthy populations. Indeed,
327 GWAS studies of the hippocampus that exclude dementia patients find little influence of AD
328 associated SNPs¹⁵. By design, nomograms are intended to model healthy progression and to
329 simplify spotting disease related outliers. Therefore, in theory, accounting for the genetics
330 of healthy variation in HV should enable earlier detection of AD-related HV decline aging
331 individuals. Conversely, stratifying by *APOE*-e4 status when creating HV nomograms charts
332 the different HV trajectories among *APOE* genotypes, however, at the same time masks the
333 pathological decline and thus will theoretically decrease the sensitivity to HV decline.

334

335 Subjects with extreme PGS account for significant amounts of the variance as indicated by
336 the S-shape in the quantile plots (e.g., Figure 3). This has been observed in other PGS-trait
337 combinations^{19,20,36}. Furthermore, we found similar R² values across all PGSs (± 0.05 R²) with
338 two peaks at thresholds of 1E-7 and 0.75. This reflects two types of genetic effects: the first
339 is that few SNPs account for a substantial portion of the total variance in HV because of
340 their high effect size (oligogenic effect) and the second is the combined effect of all
341 common genetic variants on HV (polygenic effect). This type of effect has been reported in
342 other studies of dementia³⁷.

343

344 In addition to demonstrating the clear effect of genetics on normative models, we have
345 shown GPR to be effective for estimating nomograms. Using a model-based method allows
346 us to generate accurate nomograms across the entire age range of the dataset. In fact, our
347 GPR model can potentially be extended a few years beyond those limits (Figure 2 – Figure
348 Supplement 1). In comparison, the SWA nomograms age range is reduced by 20 years

349 compared to the range of the training because of the required smoothing. Thus, compared
350 to the SWA, we extended the age range forwards by 10 years, bringing it out to 82 years old,
351 which is relevant for AD where most patients display symptoms at around age 65-75^{27,38}.
352 While some methods like LOESS regression can be used to mitigate this need³⁹, the GPR's
353 model-based approach does not need smoothing to begin with. However, there is a
354 possibility that our results suffer from edge effects. For example, we suspect that the peak
355 noted in the male nomogram is likely due to under-sampling in the younger participants.
356 We found that building nomograms is data efficient: with the SWA, using around 17% (3000
357 samples) of training samples generated nomograms that were on average only 0.4% of
358 average HV (19 mm³) different to those generated by the full training set. GPR nomograms,
359 achieved the same level of accuracy with only 5% (900 samples) of the dataset (Figure 2 –
360 Figure Supplement 3).

361

362 Using PGS improves the normative modelling in an independent dataset. In ADNI genetic
363 adjustment reduced the percentile gap between similarly diagnosed subjects with
364 genetically predicted high and low HV. The impact of the PGS adjusted model on CN
365 samples was greater than on MCI or AD samples. Genetic adjustment centred the CN
366 samples closer to the 50th percentile. As the effect of building separate nomograms was to
367 mitigate the impact of genetic variability on HV it was not surprising that this effect did not
368 carry over to MCI and AD subjects, likely because the pathological effect of AD on HV (~804
369 mm³ or 6.4% volume loss) far exceeds the shift in nomograms achieved with genetic
370 adjustment (~100 mm³ or 0.8% of mean HV). Other studies have found that annual HV loss
371 in CN subjects was between 0.38% and 1.73%^{7,40-43}. Using the nomograms from our work,
372 genetic adjustment corresponds to ~3 years of normal aging for a 65-year-old. However,
373 despite this sizable effect, genetically adjusted nomograms did not provide additional
374 insight into distinguishing MCI subjects that remained stable or converted to AD.
375 Nonetheless, the added precision may prove more useful in early detection of deviation
376 among CN subjects, for instance in detecting subtle hippocampal volume loss in individuals
377 with presymptomatic neurodegeneration.

378

379 While this study has shown the significant impact of PGSs on HV nomograms, we have
380 identified areas for improvement. Integrating the PGSs into the GP models would remove

381 the need for stratification and allow for more adjustment precision, however, PGSs are
382 prone to 'site' effects depending on the method and quality of genotyping and imputation.
383 Consequently, using the 'raw' PGSs in predictive models presents its own challenges. Also,
384 the PGSs used in this study were based on a GWAS of average bilateral HV in both male and
385 female participants. Previous studies have shown a significant difference between these
386 groups³⁰, and nomograms estimated for these separate groups are distinct^{28,44,45} (Figure 2).
387 Therefore, using separate GWASs for each of these strata would potentially give the PGSs
388 more accuracy. A second limitation of this study is the reliability of HV estimates. There is a
389 significant difference between manual and automated segmentation of the
390 hippocampus^{28,44,45}; more so than other brain regions^{46,47}, and Freesurfer is known to
391 consistently overestimate HV⁴⁸. Therefore, other brain regions with higher SNP heritability
392 like the cerebellum or whole brain volume¹⁴ may show more sensitivity on nomograms.
393 Moreover, a recent study of PGS uncertainty revealed large variance in PGS estimates⁴⁹,
394 which may undermine PGS based stratification; hence a more sophisticated method of
395 building PGS or stratification may improve results further. Finally, while NeuroCombat has
396 been shown to remove most site effects, some may remain and still need to be adjusted for
397 ⁵⁰.

398

399 In conclusion, our study demonstrated that PGS for HV was significantly positively
400 correlated with HV, translating into a shift in the nomograms corresponding to ~3 years'
401 worth of normal aging HV loss for a 65-year-old. We have additionally shown that this effect
402 can be observed in an independent dataset. And while more work in this direction is
403 needed, successful integration of polygenic effects on multiple brain regions may help
404 improve the sensitivity to detect early disease processes.

405

406

407

408

409

410

411

412

413

414

415 **Materials and Methods**

416 *Datasets*

417 Data from a total of 39,664 subjects (18,718 female) aged 44 to 82 were obtained from the
418 UKB (application number 65299) with available genotyping and imaging data. Imaging and
419 genetic protocols are described in Bycroft et al. (2018)⁵¹ and Miller et al. (2016)⁵²,
420 respectively. Briefly, for this analysis we used hippocampal volumes (HV) estimated with
421 FreeSurfer⁵³ at the initial imaging visit. The dataset preparation followed the process
422 described by Nobis et. (2019)³⁰. To ensure nomograms represent the spectrum of healthy
423 aging, subjects were excluded based on history of neurological or psychiatric disorders,
424 head trauma, substance abuse, or cardiovascular disorders. Furthermore, to control for
425 population level genetic heterogeneity, only subjects with 'British' ethnic backgrounds were
426 considered. The dataset was then stratified by self-reported sex. HV outliers were excluded
427 using mean absolute deviation (MAD) with a threshold of 5.0. Subjects' intracranial volume
428 (ICV) was derived by using the volumetric scaling from T1 head image to standard space.
429 Finally, ICV and scan date were linearly regressed out of the HVs.

430

431 For an application dataset we used the Alzheimer's Disease Neuroimaging Initiative (ADNI)
432 database (adni.loni.usc.edu)⁵⁴. The ADNI was launched in 2003 as a public-private
433 partnership, led by Principal Investigator Michael W. Weiner, MD. The primary goal of ADNI
434 has been to test whether serial magnetic resonance imaging (MRI), positron emission
435 tomography (PET), other biological markers, and clinical and neuropsychological assessment
436 can be combined to measure the progression of mild cognitive impairment (MCI) and early
437 Alzheimer's disease (AD). A total of 1001 ADNI subjects (445 male) aged 55 to 95 were
438 included in this analysis. Imaging and genetic protocols are described by Saykin et al.
439 (2010)⁵⁵ and by Jack et al. (2008)⁵⁶, respectively. Briefly, we obtained HVs estimated with
440 FreeSurfer v5.1. Subjects were excluded based on HV quality scores and based on genetic
441 ancestry (i.e., restricted to self-reported white non-Hispanic ancestry). As with UKB,
442 estimated volumes were stratified by sex, and ICV and scan date were regressed out of HV
443 estimates. Finally, we used NeuroCombat⁵⁷ to adjust across ADNI sites and harmonize the
444 volumes with the UKB Dataset. To do this we modelled 58 batches (UKB data as one batch

445 and 57 ADNI sites as separate batches) and added ICV, sex, and diagnosis (assigning all UKB
446 as Healthy and using the diagnosis columns in ADNI) to retain biological variation.
447 Demographics were obtained from the ADNIMERGE table (date accessed: 19-06-2020).
448 Furthermore, we used genotyping data of ADNI subjects pre-processed as previously
449 described by Scelsi et. (2018)⁵⁸.

450

451 *Sliding Window Approach*

452 As a baseline, we generated nomograms using the sliding window approach (SWA)
453 described by Nobis et al. (2019)³⁰. Briefly, we sorted UKB samples by age, and formed 100
454 quantile bins, each containing 10% percent of the samples. This means that neighbouring
455 bins had a 90% overlap. For example, if we had 5,000 samples, each bin contained 500
456 samples and consecutive bins were shifted by 50 samples. Thus, bin number four would
457 start at index 151. Then, within each bin, the 2.5%, 5%, 10%, 25%, 50%, 75%, 90%, 95%, and
458 97.5% quantiles were calculated. The quantiles were then smoothed with a gaussian kernel
459 of width 20. The smoothing was needed because towards the ends of the data, the sliding
460 windows approach becomes sensitive to noise.

461

462 *Gaussian Process Regression*

463 Our proposed approach uses GPR to build nomograms. Briefly, a GP is a probability
464 distribution over possible functions that fit a set of points^{59,60}. In our application it is a
465 distribution of possible ‘HV trajectories across age’. The GPR models were trained with the
466 `lap`⁶¹ R library, which implements a local approximation method that allows large
467 datasets to be trained on consumer grade machines. We applied the commonly used
468 squared exponential covariance kernel function:

$$K(x_1, x_2) = \sigma^2 e^{-\frac{(x_1 - x_2)^2}{2L^2}},$$

469 where x_1 and x_2 are any two age values from the training set. The kernel function is hyper-
470 parameterized by a vertical scale (σ) and a length scale (L), which, following initialization,
471 are fitted using maximum likelihood estimation. The vertical scale is initialized to the mean
472 HV of all samples, and the length scale is initialized to mean age difference between all
473 samples. We trained models of left, right, and mean HV for each sex. Thanks to their
474 probabilistic formulation, GP models naturally provide a standard deviation from which

475 quantiles can be easily computed. After training, we generated models for ages 45 to 82 by
476 increments of 0.25 years, and quantile curves at 2.5%, 5%, 10%, 25%, 50%, 75%, 90%, 95%,
477 and 97.5%. The UKB dataset was used to train the models and the ADNI dataset was used to
478 test them. For all GPR models, we only tested the ADNI samples that lay within the age
479 range of each model respectively.

480

481

482 *Polygenic Score for Hippocampal Volume*

483 A polygenic score (PGS) is a sum of the impact of a selection of genetic variants on a trait,
484 weighted by the allele count. That is:

$$PGS = \sum_{\forall i \in SNPs} ES_i * C_i,$$

485 where (ES_i) is the effect size (e.g., beta or log(odds) ratio from GWAS summary statistics),
486 and (C_i) is the allele count of SNP i in the subject (either 0,1 or 2). Thus, computing PGSs
487 requires SNP-level genetic data. Using a previously reported GWAS of mean bilateral HV
488 using 26,814 (European) subjects from the ENIGMA study¹⁵, we built a PGS for HV with
489 PRSice v2⁶². For both UKB and ADNI, we filter for minor allele frequency of 0.05, genotype
490 missingness of 0.1, and clumping at 250kb; after which we were left with 70,251 potential
491 SNPs to include for UKB and 114,812 for ADNI. The most widely applied strategy for SNP
492 selection is p -value thresholding. We generated PGSs at 14 p -value thresholds (1E-8, 1E-7,
493 1E-6, 1E-5, 1E-4, 1E-3, 0.01, 0.05, 0.1, 0.2, 0.4, 0.5, 0.75, 1). These thresholds produced a
494 range of polygenic scores comprising as little as 6 SNPs (p -value cut-off at 1E-8) to all
495 available SNPs (p -value cut-off at 1.0). Model fit is then checked by regressing HV against
496 these PGSs while accounting for age, age², sex, ICV, and ten genetic principal components.
497

498 *Genetically Adjusted Nomograms*

499 Given the high heritability of HV we investigated whether nomograms can be genetically
500 adjusted. Specifically, we used the top and bottom 30% samples by PGS (at p -value < 0.75
501 threshold) separately to build genetically adjusted nomograms. We found that using a 30%
502 cut-off provided a balance of training size and performance (Figure 2 – Figure Supplement
503 4). Thus, PGS provided us with a way to place new samples in their ‘appropriate’ nomogram.
504 For instance, within the ADNI dataset we generated PGSs and split the top and bottom (i.e.,

505 high, and low expected HV, respectively) to test against genetically adjusted UKB
506 nomograms. To evaluate the impact of genetic adjustment, we perform a series of ANOVA
507 tests across adjusted nomograms. E.g., we performed an ANOVA test of the HV percentiles
508 of the top 30% UKB samples in the unadjusted then the adjusted nomograms. We did the
509 same for bottom 30% and for men and women. To assess the specificity of the HV-based
510 PGS, we performed this genetic adjustment using PGSs of ICV and AD based on previously
511 reported GWASs^{63,64}.

512

513 *Longitudinal Analysis*

514 As nomograms are often used to track progression, we examined the impact of the
515 genetically adjusted nomograms on prospective longitudinal data. To this end, we analysed
516 patients from the ADNI cohort that were initially diagnosed as MCI and either converted to
517 AD (progressor) or remained MCI (stable) within five years of follow-up. We tested whether
518 the PGS-adjusted nomograms improved the separation between stable and progressor
519 patients using Cox proportional hazards models while accounting for sex and age.

520

521 **Code and Data Availability**

522 The scripts and code used in this study have been made publicly available and can be found
523 at: <https://github.com/Mo-Janahi/NOMOGRAMS>. All underlying data, and derived
524 quantities, are available by application from the UK Biobank at
525 <http://www.ukbiobank.ac.uk>, and by application from ADNI at
526 <http://adni.loni.usc.edu/data-samples/access-data/>. Summary statistics from all genome-
527 wide association studies described in this paper are available from the NHGRI-EBI GWAS
528 catalog, study numbers: GCST003834, GCST002245, and GCST003961. URL:
529 <https://www.ebi.ac.uk/gwas/studies/>

530

531 **Ethics Statement**

532 This work uses exclusively pseudonymized data that were collected as part of different
533 studies (ADNI and UKB). Research ethics approval was granted by UCL as part of project
534 #13083/002.

535

536 **Competing Interests**

537 No potential competing interest was reported by the authors.

538

539 **Acknowledgements**

540 AA holds an MRC eMedLab Medical Bioinformatics Career Development Fellowship. This
541 work was supported by the Medical Research Council [grant number MR/L016311/1]. This
542 work was supported in part by Sidra Medicine, Qatar. LMA was supported by the National
543 Institute of Biomedical Imaging and Bioengineering of the National Institutes of Health
544 under Award Number P41EB015922 and by the National Institute on Aging of the National
545 Institutes of Health under Award Number P30AG066530. JMS acknowledges the support of
546 the UCL/H NIHR Biomedical Research Centre. This work is supported by the EPSRC-funded
547 UCL Centre for Doctoral Training in Intelligent, Integrated Imaging in Healthcare (i4health)
548 [EP/S021930/1].

549 Data used in preparation of this article were obtained from the Alzheimer's Disease
550 Neuroimaging Initiative (ADNI) database (adni.loni.ucla.edu). Data collection and sharing for
551 this project was funded by the Alzheimer's Disease Neuroimaging Initiative (ADNI) (National
552 Institutes of Health Grant U01 AG024904) and DOD ADNI (Department of Defense award
553 number W81XWH-12-2-0012). ADNI is funded by the National Institute on Aging, the
554 National Institute of Biomedical Imaging and Bioengineering, and through generous
555 contributions from the following: AbbVie, Alzheimer's Association; Alzheimer's Drug
556 Discovery Foundation; Araclon Biotech; BioClinica, Inc.; Biogen; Bristol-Myers Squibb
557 Company; CereSpir, Inc.; Cogstate; Eisai Inc.; Elan Pharmaceuticals, Inc.; Eli Lilly and
558 Company; EuroImmun; F. Hoffmann-La Roche Ltd and its affiliated company Genentech,
559 Inc.; Fujirebio; GE Healthcare; IXICO Ltd.; Janssen Alzheimer Immunotherapy Research &
560 Development, LLC.; Johnson & Johnson Pharmaceutical Research & Development LLC.;
561 Lumosity; Lundbeck; Merck & Co., Inc.; Meso Scale Diagnostics, LLC.; NeuroRx Research;
562 Neurotrack Technologies; Novartis Pharmaceuticals Corporation; Pfizer Inc.; Piramal
563 Imaging; Servier; Takeda Pharmaceutical Company; and Transition Therapeutics. The
564 Canadian Institutes of Health Research is providing funds to support ADNI clinical sites in
565 Canada. Private sector contributions are facilitated by the Foundation for the National
566 Institutes of Health (www.fnih.org). The grantee organization is the Northern California
567 Institute for Research and Education, and the study is coordinated by the Alzheimer's

568 Therapeutic Research Institute at the University of Southern California. ADNI data are
569 disseminated by the Laboratory for Neuro Imaging at the University of Southern California.
570 As such, the investigators within the ADNI contributed to the design and implementation of
571 ADNI and/or provided data but did not participate in analysis or writing of this report.

572 **Supplementary Figure Legends:**

573

574 **Figure 2 – Figure Supplement 1: Expanded GPR Nomogram.** a GPR model trained with
575 mean bilateral HV of male subjects in the age range 45-82 (grey circles) and then generated
576 nomograms for the age range 30-100. Within training data range nomogram follows data
577 reasonably well. Outside data range, nomogram flairs out from expected range after 2-6
578 years. Fairing is faster in the lower ages because, outside the data range, the GPR model
579 reverts to a normal distribution with zero mean. For all sub-figures, the black lines -from top
580 to bottom-represent the 2.5%, 5%, 10%, 25%, 50%, 75%, 90%, 95%, and 97.5% quantiles
581 respectively.

582

583 **Figure 2 – Figure Supplement 2: Model fit of healthy ADNI subjects.** Nomograms produced
584 from healthy subjects in the UKB using the gaussian process regression (GPR) method.
585 Overlaid are scatter plots Cognitively Normal subjects from the ADNI dataset. Male
586 subjects averaged ($56.9\% \pm 24.6$ SD) and Female subjects averaged (54.9 ± 26.5 SD). For
587 both sub-figures, the black lines -from top to bottom-represent the 2.5%, 5%, 10%, 25%,
588 50%, 75%, 90%, 95%, and 97.5% quantiles respectively.

589 **Figure 2 – Figure Supplement 3: Performance of GPR and SWM across sample size.** Model
590 training progression is shown for both SWM (top row) and GPR (middle row) models at
591 representative training sizes. Performance (bottom figure) is summarized using the mean
592 distance between generated nomograms and the GPR nomograms built with the full
593 training set (~15k) (shaded areas in the top two rows). By repeatedly sampling data from
594 across age (10 times at each training sample size), we plot the average performance and
595 95% CI of each method. Both methods are data efficient, SWM can achieve 20 mm³ mean
596 difference (0.4% of mean HV) performance using ~3000 samples (20% of training set), and
597 GPR can achieve the same performance using only 1000 samples (~7% of training set).

598 **Figure 2 – Figure Supplement 4: GPR model across top/bottom thresholds.** Illustrated is
599 Male bilateral HV. When stratifying by PRS, there is a trade-off between training set size and
600 final model performance. In these figures, performance is measured by average distance
601 between the percentile curves. At 10%, (leftmost column), the top/bottom strata contain
602 ~1500 samples each and the mean distance is 65 mm³, and at 50% (the rightmost column)
603 they contain ~7500 and the mean distance is 21.5 mm³. For all sub-figures, the black lines -
604 from top to bottom-represent the 2.5%, 5%, 10%, 25%, 50%, 75%, 90%, 95%, and 97.5%
605 quantiles respectively.

606

607 **Figure 3 – Figure Supplement 1: Summary of PGSs based on HV GWAS in UKB samples.** The
608 left set of graphs show the R-Squared of the regression models of PRS across HV for the

609 scores built across SNP P-Value thresholds. While the difference is small, we consistently see
610 a dip in the R-Squared for the middle set of thresholds. The set of figures to the right show
611 the spread of HV across PRS percentile. We display the percentiles for the 0.75 threshold as
612 it showed the best correlation with HV overall.

613

614 **Figure 3 – Figure Supplement 2: Summary of PGSs and models based on HV GWAS and**
615 **ADNI samples.** The left set of graphs show the R-Squared of the regression models of PRS
616 across HV for the scores built across SNP P-Value thresholds. In contrast to the graphs seen
617 in the UKB samples, the R-squared values for the most part increase with p-value threshold.
618 The set of graphs on the right show the spread of HV across PGS percentiles, each at the
619 score that had the highest R-Squared value from the corresponding left graph.
620

621 **Figure 4 – Figure Supplement 1: Genetically Adjusted Nomograms.** For all sub-figures, the
622 black lines -from top to bottom-represent the 2.5%, 5%, 10%, 25%, 50%, 75%, 90%, 95%,
623 and 97.5% quantiles respectively.

624 **Figure 4 – Figure Supplement 2:** Nomograms generated with the SWM by stratifying the
625 sample set based on PGSs. Left column: PGS based on HV GWAS. Middle column: PGS based
626 on ICV GWAS. Right column: PGS based on AD GWAS. For all sub-figures, the black lines -
627 from top to bottom-represent the 2.5%, 5%, 10%, 25%, 50%, 75%, 90%, 95%, and 97.5%
628 quantiles respectively.

629 **Figure 4 – Figure Supplement 3: Training Data Ridge Plots.** Histograms of bilateral HV
630 across the different subsets of the datasets. Samples are grouped in bins of 5 years. N is the
631 number of samples in each set and p is the p-value from a Shapiro-Wilks test of normality.
632 Typically, this test would indicate a non-gaussian distribution with a p-value lower than 0.05
633 (0.001 corrected for 48 multiple tests in this case).
634

635

636

637

637 References

638

- 639 1. Shen L, Thompson PM. Brain Imaging Genomics: Integrated Analysis and Machine
640 Learning. *Proceedings of the IEEE*. 2020;108(1):125-162. doi:10.1109/JPROC.2019.2947272
- 641 2. Marquand AF, Rezek I, Buitelaar J, Beckmann CF. Understanding Heterogeneity in
642 Clinical Cohorts Using Normative Models: Beyond Case-Control Studies. *Biological*
643 *Psychiatry*. 2016;80(7):552-561. doi:10.1016/j.biopsych.2015.12.023
- 644 3. Pinaya WHL, Scarpazza C, Garcia-Dias R, et al. Normative modelling using deep
645 autoencoders: A multi-cohort study on mild cognitive impairment and Alzheimer's disease.
646 bioRxiv; 2020. p. 2020.02.10.931824-2020.02.10.931824.
- 647 4. Wolfers T, Beckmann CF, Hoogman M, Buitelaar JK, Franke B, Marquand AF.
648 Individual differences v. the average patient: Mapping the heterogeneity in ADHD using
649 normative models. *Psychological Medicine*. 2019;50(2):314-323.
650 doi:10.1017/S0033291719000084

- 651 5. Ziegler G, Ridgway GR, Dahnke R, Gaser C. Individualized Gaussian process-based
652 prediction and detection of local and global gray matter abnormalities in elderly subjects.
653 *NeuroImage*. 2014;97:333-348. doi:10.1016/j.neuroimage.2014.04.018
- 654 6. Xavier Castellanos F, Lee PP, Sharp W, et al. Developmental trajectories of brain
655 volume abnormalities in children and adolescents with attention-deficit/hyperactivity
656 disorder. *Journal of the American Medical Association*. 2002;288(14):1740-1748.
657 doi:10.1001/jama.288.14.1740
- 658 7. Scahill RI, Frost C, Jenkins R, Whitwell JL, Rossor MN, Fox NC. A longitudinal study of
659 brain volume changes in normal aging using serial registered magnetic resonance imaging.
660 *Archives of Neurology*. 2003;60(7):989-994. doi:10.1001/archneur.60.7.989
- 661 8. Peterson M, Warf BC, Schiff SJ. Normative human brain volume growth. *Journal of*
662 *Neurosurgery: Pediatrics*. 2018;21(5):478-485. doi:10.3171/2017.10.PEDS17141
- 663 9. Lukies MW, Watanabe Y, Tanaka H, et al. Heritability of brain volume on MRI in
664 middle to advanced age: A twin study of Japanese adults. *PLoS ONE*.
665 2017;12(4)doi:10.1371/journal.pone.0175800
- 666 10. Kremen WS, Prom-Wormley E, Panizzon MS, et al. Genetic and environmental
667 influences on the size of specific brain regions in midlife: The VETSA MRI study. *NeuroImage*.
668 2010-01-01 2010;49(2):1213-1223. doi:10.1016/j.neuroimage.2009.09.043
- 669 11. Thompson PM, Jahanshad N, Ching CRK, et al. ENIGMA and global neuroscience: A
670 decade of large-scale studies of the brain in health and disease across more than 40
671 countries. Springer Nature; 2020. p. 1-28.
- 672 12. Hibar DP, Stein JL, Renteria ME, et al. Common genetic variants influence human
673 subcortical brain structures. *Nature*. 2015-04-01 2015;520(7546):224-229.
674 doi:10.1038/nature14101
- 675 13. Rentería ME, Hansell NK, Strike LT, et al. Genetic architecture of subcortical brain
676 regions: Common and region-specific genetic contributions. *Genes, Brain and Behavior*.
677 2014;13(8):821-830. doi:10.1111/gbb.12177
- 678 14. Zhao B, Ibrahim JG, Li Y, et al. Heritability of Regional Brain Volumes in Large-Scale
679 Neuroimaging and Genetic Studies. *Cerebral Cortex*. 2019;29(7):2904-2914.
680 doi:10.1093/cercor/bhy157
- 681 15. Hibar DP, Adams HHH, Jahanshad N, et al. Novel genetic loci associated with
682 hippocampal volume. *Nature Communications*. 2017;8doi:10.1038/ncomms13624
- 683 16. Grasby KL, Jahanshad N, Painter JN, et al. The genetic architecture of the human
684 cerebral cortex. *Science*. 2020-03-20 2020;367(6484):eaay6690.
685 doi:10.1126/science.aay6690
- 686 17. Manolio TA, Collins FS, Cox NJ, et al. Finding the missing heritability of complex
687 diseases. *Nature*. 2009-10-01 2009;461(7265):747-753. doi:10.1038/nature08494
- 688 18. Foo H, Thalamuthu A, Jiang J, et al. Associations between Alzheimer's disease
689 polygenic risk scores and hippocampal subfield volumes in 17,161 UK Biobank participants.
690 *Neurobiology of Aging*. 2021;98:108-115. doi:10.1016/j.neurobiolaging.2020.11.002
- 691 19. Axelrud LK, Santoro ML, Pine DS, et al. Polygenic risk score for Alzheimer's disease:
692 Implications for memory performance and hippocampal volumes in early life. *American*
693 *Journal of Psychiatry*. 2018;175(6):555-563. doi:10.1176/appi.ajp.2017.17050529
- 694 20. Escott-Price V, Nalls MA, Morris HR, et al. Polygenic risk of P arkinson
695 disease is correlated with disease age at onset. *Annals of Neurology*. 2015;77(4):582-591.
696 doi:10.1002/ana.24335

- 697 21. Bird CM, Burgess N. The hippocampus and memory: Insights from spatial processing.
698 Nature Publishing Group; 2008. p. 182-194.
- 699 22. Bremner JD, Narayan M, Anderson ER, Staib LH, Miller HL, Charney DS. Hippocampal
700 Volume Reduction in Major Depression. *American Journal of Psychiatry*. 2000-01-01
701 2000;157(1):115-118. doi:10.1176/ajp.157.1.115
- 702 23. Nelson MD, Saykin AJ, Flashman LA, Riordan HJ. Hippocampal Volume Reduction in
703 Schizophrenia as Assessed by Magnetic Resonance Imaging. *Archives of General Psychiatry*.
704 1998-05-01 1998;55(5):433. doi:10.1001/archpsyc.55.5.433
- 705 24. Whelan CD, Altmann A, Botía JA, et al. Structural brain abnormalities in the common
706 epilepsies assessed in a worldwide ENIGMA study. *Brain : a journal of neurology*.
707 2018;141(2):391-408. doi:10.1093/brain/awx341
- 708 25. Pini L, Pievani M, Bocchetta M, et al. Brain atrophy in Alzheimer's Disease and aging.
709 *Ageing Research Reviews*. 2016-09-01 2016;30:25-48. doi:10.1016/j.arr.2016.01.002
- 710 26. Van Der Flier WM, Scheltens P. Epidemiology and risk factors of dementia. BMJ
711 Publishing Group Ltd; 2005. p. 2-7.
- 712 27. Rabinovici GD. Late-onset Alzheimer disease. Lippincott Williams and Wilkins; 2019.
713 p. 14-33.
- 714 28. Schmidt MF, Storrs JM, Freeman KB, et al. A comparison of manual tracing and
715 FreeSurfer for estimating hippocampal volume over the adult lifespan. *Human Brain*
716 *Mapping*. 2018;39(6):2500-2513. doi:10.1002/hbm.24017
- 717 29. Fraser MA, Shaw ME, Cherbuin N. A systematic review and meta-analysis of
718 longitudinal hippocampal atrophy in healthy human ageing. Academic Press Inc.; 2015. p.
719 364-374.
- 720 30. Nobis L, Manohar SG, Smith SM, et al. Hippocampal volume across age: Nomograms
721 derived from over 19,700 people in UK Biobank. *NeuroImage: Clinical*.
722 2019;23doi:10.1016/j.nicl.2019.101904
- 723 31. Mather KA, Armstrong NJ, Wen W, et al. Investigating the Genetics of Hippocampal
724 Volume in Older Adults without Dementia. *PLOS ONE*. 2015-01-27 2015;10(1):e0116920.
725 doi:10.1371/journal.pone.0116920
- 726 32. Ching C, Abaryan Z, Santhalingam V, et al. Sex differences in subcortical aging: A
727 nomogram study of age, sex, and apoe (N = 9,414). *Alzheimer's & Dementia*.
728 2020;16(S4):e045774-e045774. doi:10.1002/alz.045774
- 729 33. Veldsman M, Nobis L, Alfaro-Almagro F, Manohar S, Husain M. The human
730 hippocampus and its subfield volumes across age, sex and APOE e4 status. *Brain*
731 *Communications*. 2021;3(1)doi:10.1093/braincomms/fcaa219
- 732 34. Kim J, Basak JM, Holtzman DM. The Role of Apolipoprotein E in Alzheimer's Disease.
733 NIH Public Access; 2009. p. 287-303.
- 734 35. Liu CC, Kanekiyo T, Xu H, Bu G. Apolipoprotein e and Alzheimer disease: Risk,
735 mechanisms and therapy. NIH Public Access; 2013. p. 106-118.
- 736 36. Ranlund S, Calafato S, Thygesen JH, et al. A polygenic risk score analysis of psychosis
737 endophenotypes across brain functional, structural, and cognitive domains. *American*
738 *Journal of Medical Genetics Part B: Neuropsychiatric Genetics*. 2018;177(1):21-34.
739 doi:10.1002/ajmg.b.32581
- 740 37. Bis JC, Decarli C, Smith AV, et al. Common variants at 12q14 and 12q24 are
741 associated with hippocampal volume. *Nature Genetics*. 2012;44(5):545-551.
742 doi:10.1038/ng.2237
- 743 38. Mendez MF. Early-Onset Alzheimer Disease. W.B. Saunders; 2017. p. 263-281.

744 39. Bethlehem RAI, Seidlitz J, Romero-Garcia R, Trakoshis S, Dumas G, Lombardo MV. A
745 normative modelling approach reveals age-atypical cortical thickness in a subgroup of males
746 with autism spectrum disorder. *Communications Biology*. 2020-12-01
747 2020;3(1)doi:10.1038/s42003-020-01212-9

748 40. Leong RLF, Lo JC, Sim SKY, et al. Longitudinal brain structure and cognitive changes
749 over 8 years in an East Asian cohort. *NeuroImage*. 2017;147:852-860.
750 doi:10.1016/j.neuroimage.2016.10.016

751 41. Jack CR, Petersen RC, Xu Y, et al. Rates of hippocampal atrophy correlate with
752 change in clinical status in aging and AD. *Neurology*. 2000;55(4):484-489.
753 doi:10.1212/wnl.55.4.484

754 42. Mori E, Lee K, Yasuda M, et al. Accelerated hippocampal atrophy in Alzheimer's
755 disease with apolipoprotein E ϵ 4 allele. *Annals of Neurology*. 2002-02-01 2002;51(2):209-
756 214. doi:10.1002/ana.10093

757 43. Risacher SL, Shen L, West JD, et al. Longitudinal MRI atrophy biomarkers:
758 Relationship to conversion in the ADNI cohort. *Neurobiology of Aging*. 2010-08-01
759 2010;31(8):1401-1418. doi:10.1016/j.neurobiolaging.2010.04.029

760 44. Khlif MS, Egorova N, Werden E, et al. A comparison of automated segmentation and
761 manual tracing in estimating hippocampal volume in ischemic stroke and healthy control
762 participants. *NeuroImage: Clinical*. 2019;21:101581-101581. doi:10.1016/j.nicl.2018.10.019

763 45. Pardoe HR, Pell GS, Abbott DF, Jackson GD. Hippocampal volume assessment in
764 temporal lobe epilepsy: How good is automated segmentation? *Epilepsia*.
765 2009;50(12):2586-2592. doi:10.1111/j.1528-1167.2009.02243.x

766 46. Keller SS, Gerdes JS, Mohammadi S, et al. Volume estimation of the thalamus using
767 FreeSurfer and stereology: Consistency between methods. *Neuroinformatics*.
768 2012;10(4):341-350. doi:10.1007/s12021-012-9147-0

769 47. Buser NJ, Madan CR, Hanson JL. Quantifying numerical and spatial reliability of
770 amygdala and hippocampal subdivisions in FreeSurfer. *bioRxiv*; 2020. p. 2020.06.12.149203-
771 2020.06.12.149203.

772 48. Perlaki G, Horvath R, Nagy SA, et al. Comparison of accuracy between FSL's FIRST and
773 Freesurfer for caudate nucleus and putamen segmentation. *Scientific Reports*. 2017;7(1):1-
774 9. doi:10.1038/s41598-017-02584-5

775 49. Ding Y, Hou K, Burch KS, et al. Large uncertainty in individual PRS estimation impacts
776 PRS-based risk stratification. *bioRxiv*; 2020. p. 2020.11.30.403188-2020.11.30.403188.

777 50. Stamoulou E, Manikis GC, Tsiknakis M, Marias K. ComBat harmonization for
778 multicenter MRI based radiomics features. *IEEE*; 2021:

779 51. Bycroft C, Freeman C, Petkova D, et al. The UK Biobank resource with deep
780 phenotyping and genomic data. *Nature*. 2018;562(7726):203-209. doi:10.1038/s41586-018-
781 0579-z

782 52. Miller KL, Alfaro-Almagro F, Bangerter NK, et al. Multimodal population brain
783 imaging in the UK Biobank prospective epidemiological study. *Nature Neuroscience*.
784 2016;19(11):1523-1536. doi:10.1038/nn.4393

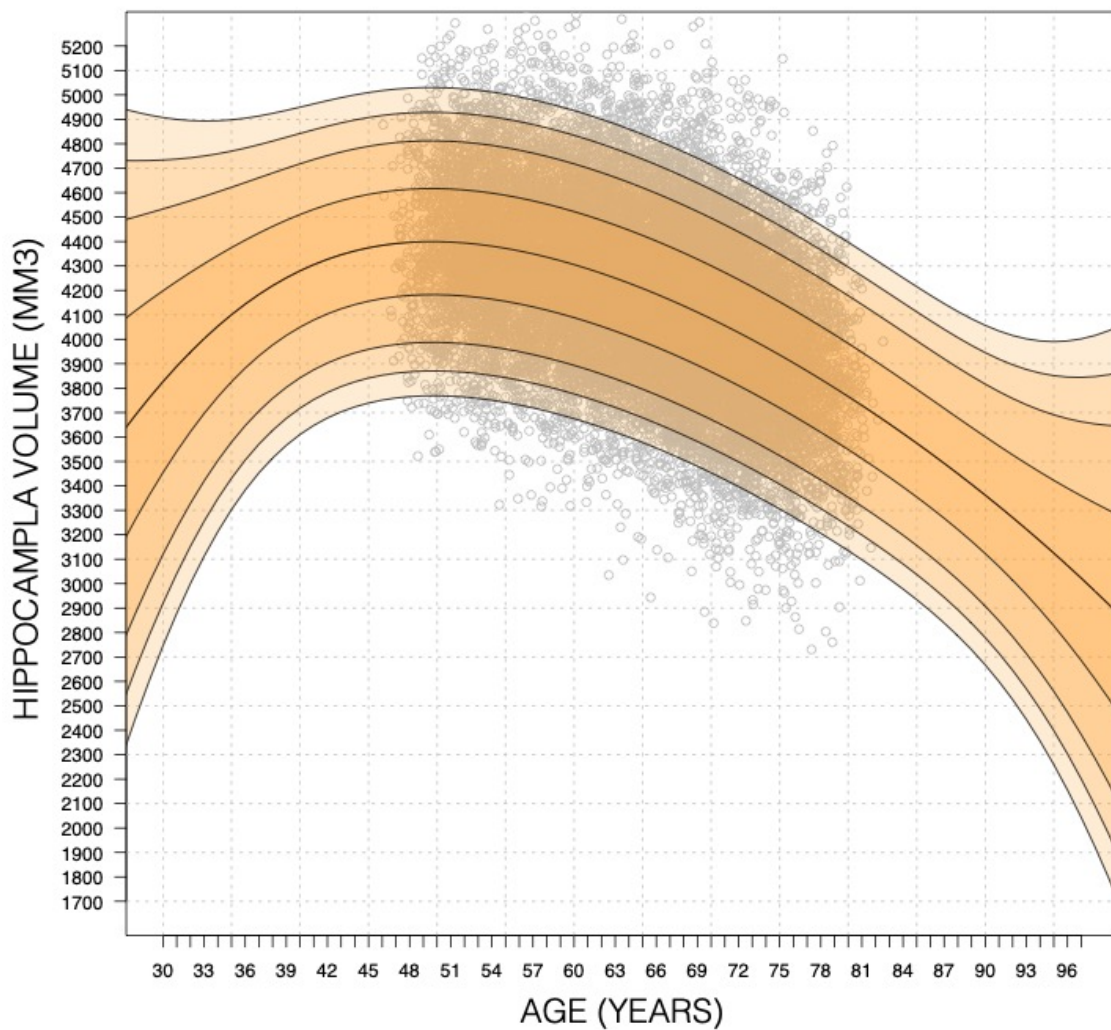
785 53. Fischl B. FreeSurfer. NIH Public Access; 2012. p. 774-781.

786 54. Petersen RC, Aisen PS, Beckett LA, et al. Alzheimer's Disease Neuroimaging Initiative
787 (ADNI): Clinical characterization. *Neurology*. 2010;74(3):201-209.
788 doi:10.1212/WNL.0b013e3181cb3e25

789 55. Saykin AJ, Shen L, Foroud TM, et al. Alzheimer's Disease Neuroimaging Initiative
790 biomarkers as quantitative phenotypes: Genetics core aims, progress, and plans. *Alzheimer's*
791 *and Dementia*. 2010;6(3):265-273. doi:10.1016/j.jalz.2010.03.013
792 56. Jack CR, Bernstein MA, Fox NC, et al. The Alzheimer's disease neuroimaging initiative
793 (ADNI): MRI methods. *Journal of Magnetic Resonance Imaging*. 2008;27(4):685-691.
794 doi:10.1002/jmri.21049
795 57. Fortin JP, Cullen N, Sheline YI, et al. Harmonization of cortical thickness
796 measurements across scanners and sites. *NeuroImage*. 2018;167:104-120.
797 doi:10.1016/j.neuroimage.2017.11.024
798 58. Scelsi MA, Khan RR, Lorenzi M, et al. Genetic study of multimodal imaging
799 Alzheimer's disease progression score implicates novel loci. *Brain*. 2018;141(7):2167-2180.
800 doi:10.1093/brain/awy141
801 59. Rasmussen CE, Williams CKI. *Gaussian Processes for Machine Learning*. 2006.
802 026218253X. www.GaussianProcess.org/gpml
803 60. Wang J. *An Intuitive Tutorial to Gaussian Processes Regression*. 2021.
804 61. Gramacy RB. LaGP: Large-scale spatial modeling via local approximate Gaussian
805 processes in R. *Journal of Statistical Software*. 2016;72(1):1-46. doi:10.18637/jss.v072.i01
806 62. Choi SW, O'Reilly PF. PRSice-2: Polygenic Risk Score software for biobank-scale data.
807 *GigaScience*. 2019;8(7):1-6. doi:10.1093/gigascience/giz082
808 63. Adams HHH, Hibar DP, Chouraki V, et al. Novel genetic loci underlying human
809 intracranial volume identified through genome-wide association. *Nature Neuroscience*.
810 2016;19(12):1569-1582. doi:10.1038/nn.4398
811 64. Lambert JC, Ibrahim-Verbaas CA, Harold D, et al. Meta-analysis of 74,046 individuals
812 identifies 11 new susceptibility loci for Alzheimer's disease. *Nature Genetics*.
813 2013;45(12):1452-1458. doi:10.1038/ng.2802
814
815
816
817
818
819
820
821
822
823
824
825
826
827

828 **Supplementary Figures**

829 **MALE BILATERAL HV**



863 **Figure 2 – Figure Supplement 1: Expanded GPR Nomogram.** a GPR model trained with
864 mean bilateral HV of male subjects in the age range 45-82 (grey circles) and then generated
865 nomograms for the age range 30-100. Within training data range nomogram follows data
866 reasonably well. Outside data range, nomogram flairs out from expected range after 2-6
867 years. Fairing is faster in the lower ages because, outside the data range, the GPR model
868 reverts to a normal distribution with zero mean. For all sub-figures, the black lines -from top to bottom-
869 represent the 2.5%, 5%, 10%, 25%, 50%, 75%, 90%, 95%, and 97.5% quantiles
870 respectively.

871
872
873
874

875
876
877
878
879
880
881
882
883
884
885
886
887
888
889
890
891
892
893
894
895
896
897
898
899
900
901
902
903
904
905
906
907
908
909
910
911
912
913
914
915
916
917
918
919
920
921

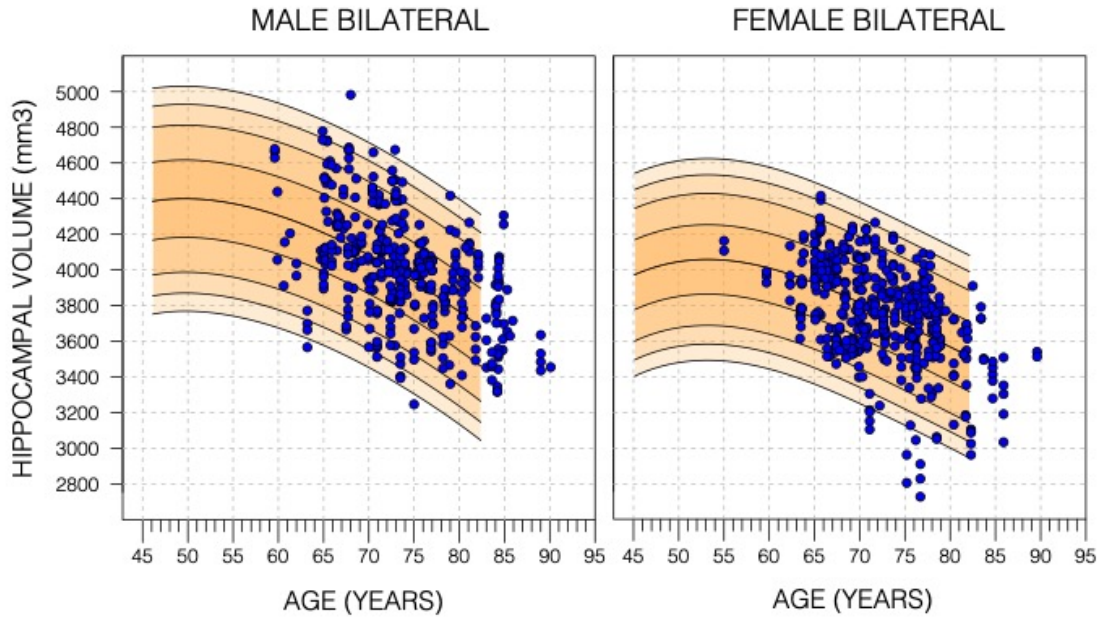
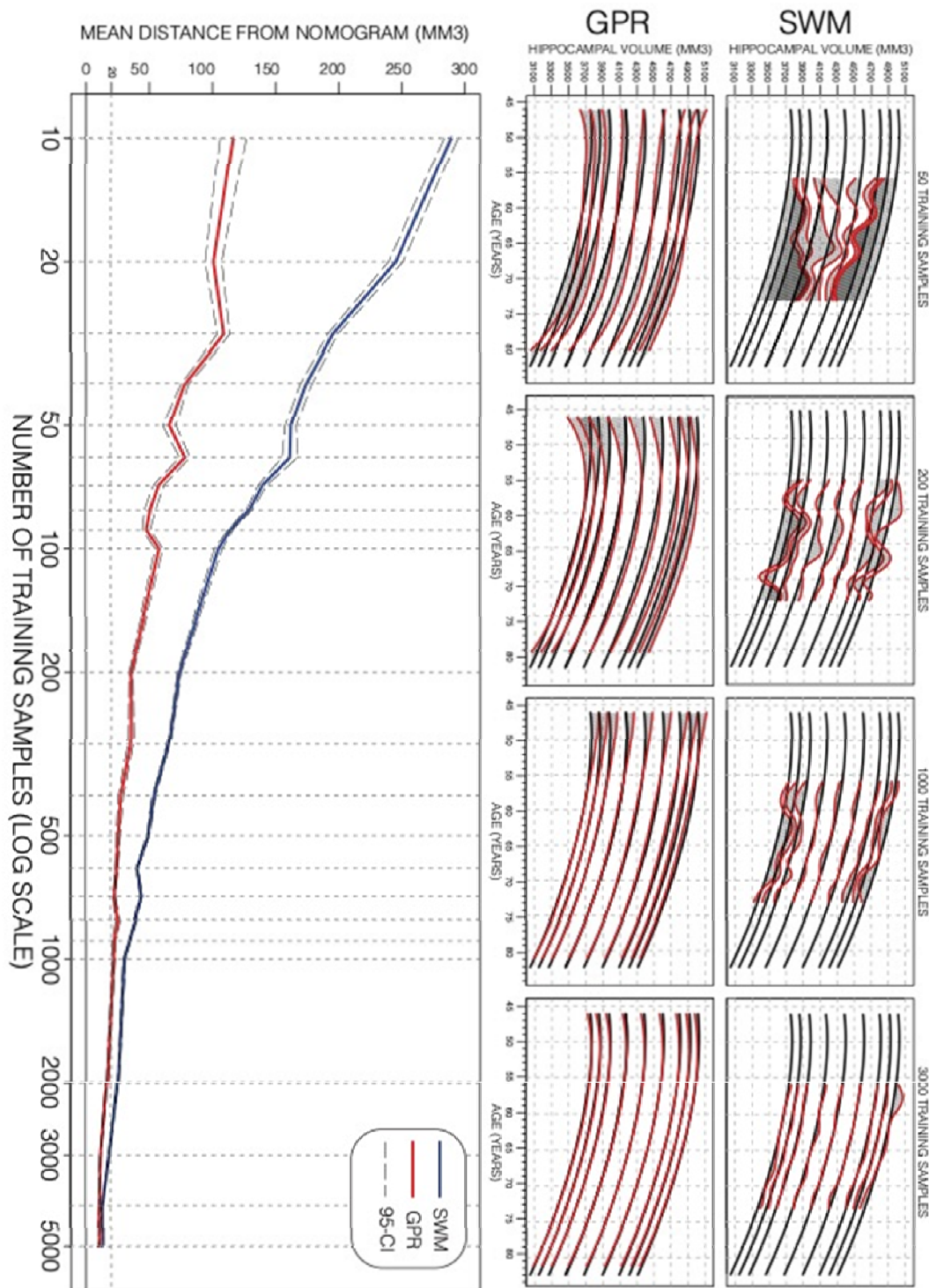


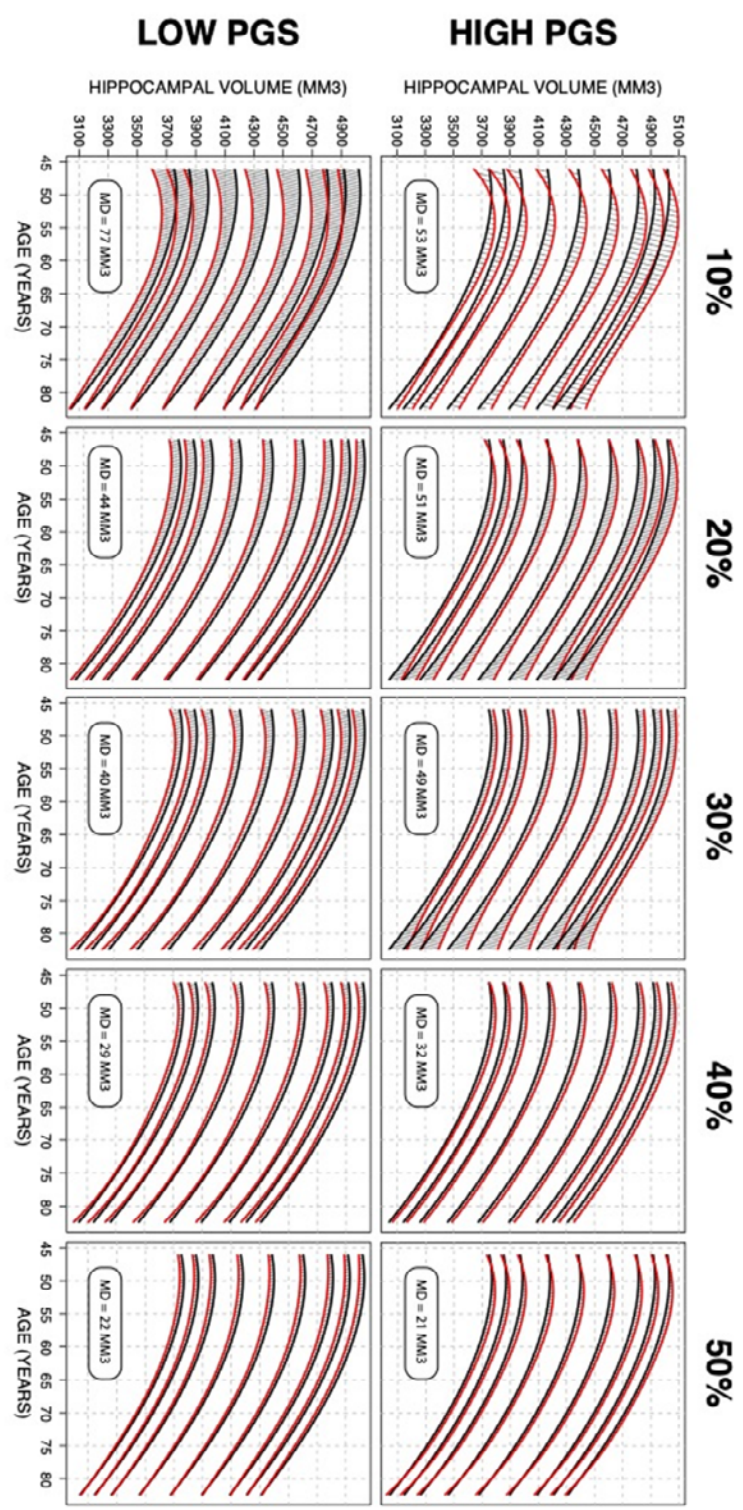
Figure 2 – Figure Supplement 2: Model fit of healthy ADNI subjects. Nomograms produced from healthy subjects in the UKB using the gaussian process regression (GPR) method. Overlaid are scatter plots Cognitively Normal subjects from the ADNI dataset. Male subjects averaged ($56.9\% \pm 24.6$ SD) and Female subjects averaged (54.9 ± 26.5 SD). For both sub-figures, the black lines -from top to bottom-represent the 2.5%, 5%, 10%, 25%, 50%, 75%, 90%, 95%, and 97.5% quantiles respectively.



922
923
924
925
926
927
928
929
930
931
932
933
934
935
936
937
938
939
940
941
942
943
944
945
946
947
948
949
950
951
952
953
954
955
956
957
958

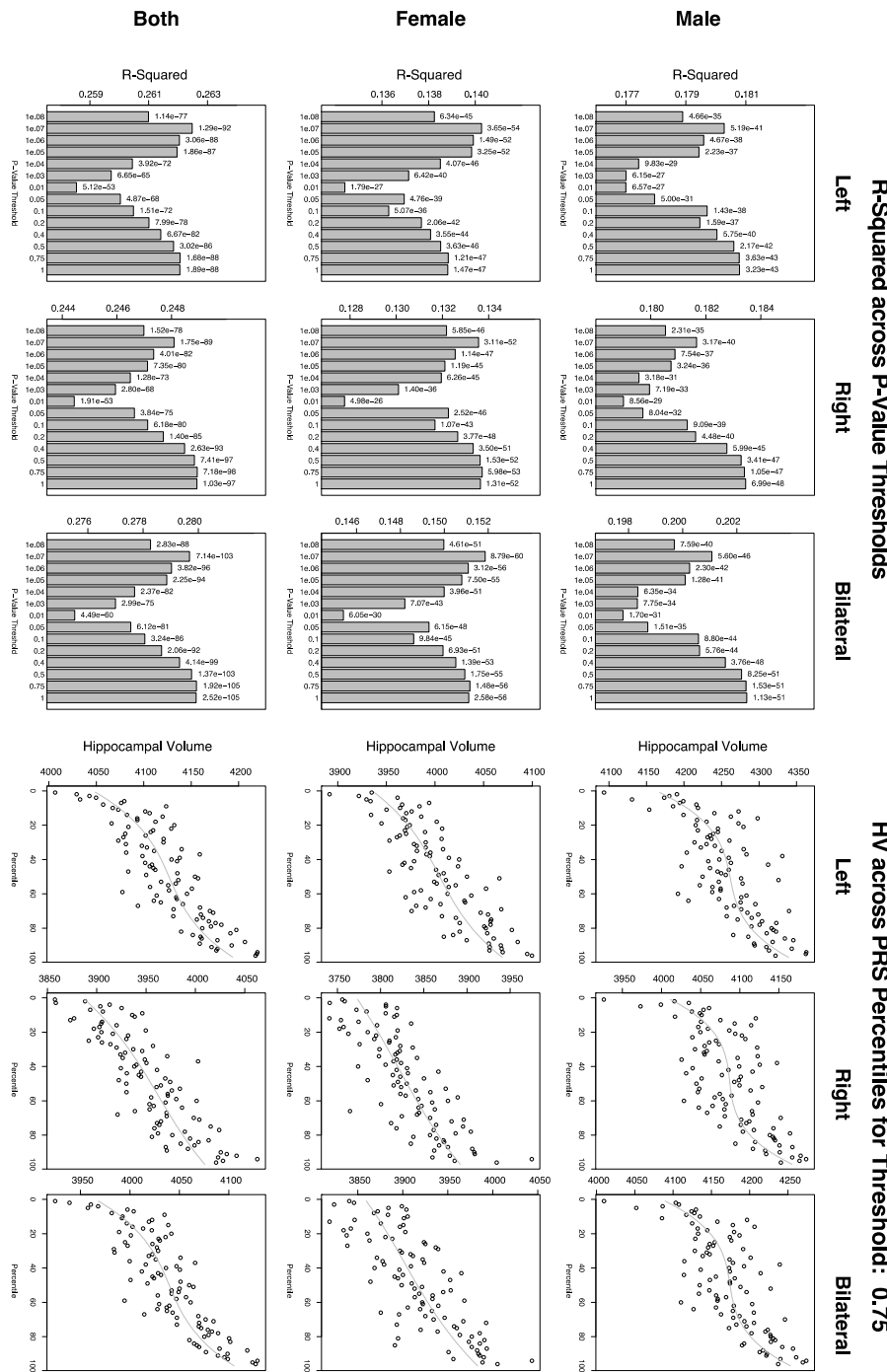
959 **Figure 2 – Figure Supplement 3: Performance of GPR and SWM across sample size.** Model
960 training progression is shown for both SWM (top row) and GPR (middle row) models at
961 representative training sizes. Performance (bottom figure) is summarized using the mean
962 distance between generated nomograms and the GPR nomograms built with the full
963 training set (~15k) (shaded areas in the top two rows). By repeatedly sampling data from
964 across age (10 times at each training sample size), we plot the average performance and
965 95% CI of each method. Both methods are data efficient, SWM can achieve 20 mm³ mean
966 difference (0.4% of mean HV) performance using ~3000 samples (20% of training set), and
967 GPR can achieve the same performance using only 1000 samples (~7% of training set).

968
969
970
971
972
973
974
975
976
977
978
979
980
981
982
983
984
985
986
987
988
989
990
991
992
993
994
995
996
997
998
999
1000
1001
1002
1003
1004



1005 **Figure 2 – Figure Supplement 4: GPR model across top/bottom thresholds.** Illustrated is
 1006 Male bilateral HV. When stratifying by PRS, there is a trade-off between training set size and
 1007 final model performance. In these figures, performance is measured by average distance
 1008 between the percentile curves. At 10%, (leftmost column), the top/bottom strata contain
 1009 ~1500 samples each and the mean distance is 65 mm³, and at 50% (the rightmost column)
 1010 they contain ~7500 and the mean distance is 21.5 mm³. For all sub-figures, the black lines -
 1011 from top to bottom-represent the 2.5%, 5%, 10%, 25%, 50%, 75%, 90%, 95%, and 97.5%
 1012 quantiles respectively.

1013
 1014
 1015
 1016
 1017
 1018
 1019
 1020
 1021
 1022
 1023
 1024
 1025
 1026
 1027
 1028
 1029
 1030
 1031
 1032
 1033
 1034
 1035
 1036
 1037
 1038
 1039



1040 **Figure 3 – Figure Supplement 1: Summary of PGSs based on HV GWAS in UKB samples.** The
 1041 left set of graphs show the R-Squared of the regression models of PRS across HV for the
 1042 scores built across SNP P-Value thresholds. While the difference is small, we consistently see
 1043 a dip in the R-Squared for the middle set of thresholds. The set of figures to the right show
 1044 the spread of HV across PRS percentiles. We display the percentiles for the 0.75 threshold as
 1045 it showed the best correlation with HV overall.

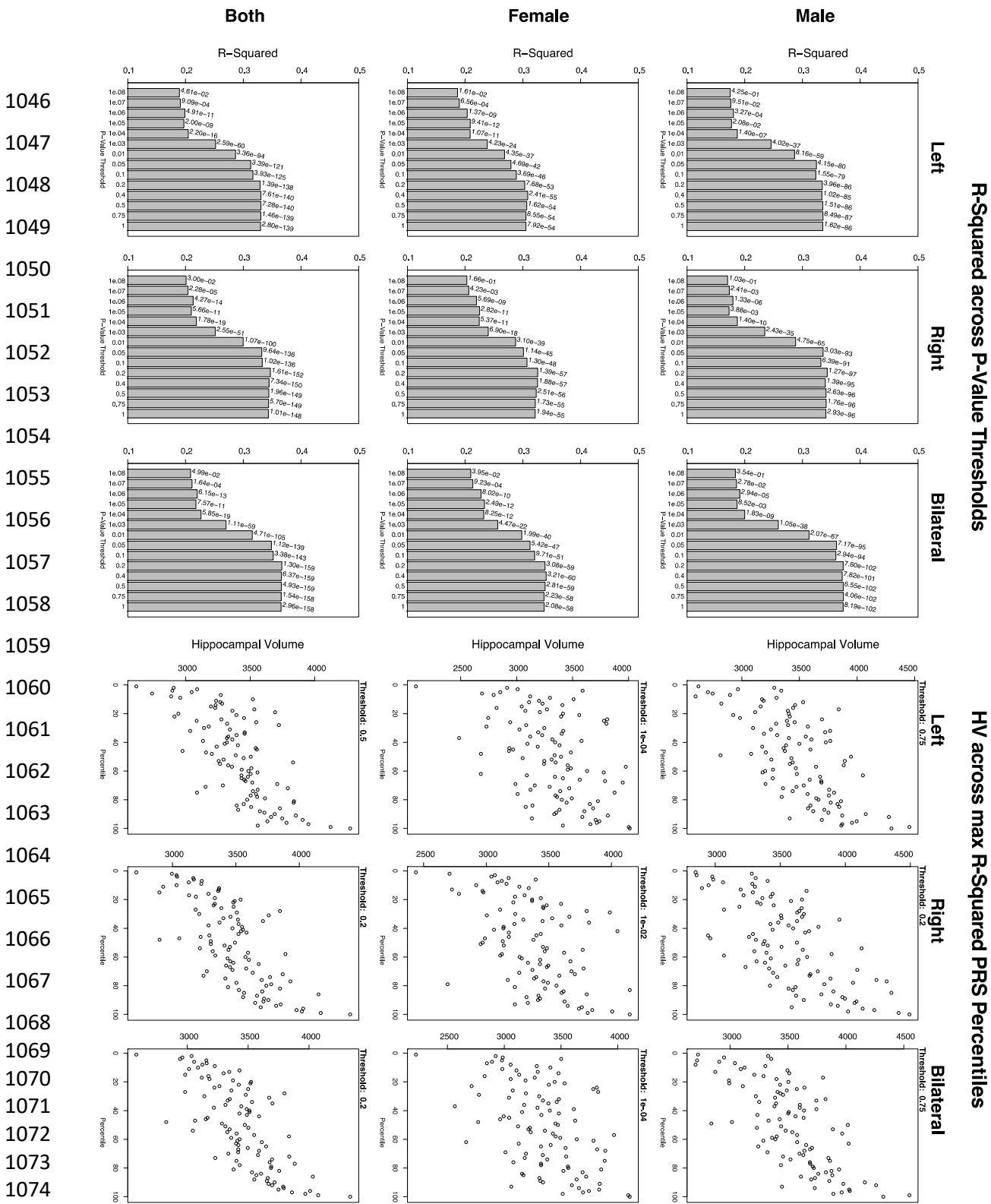
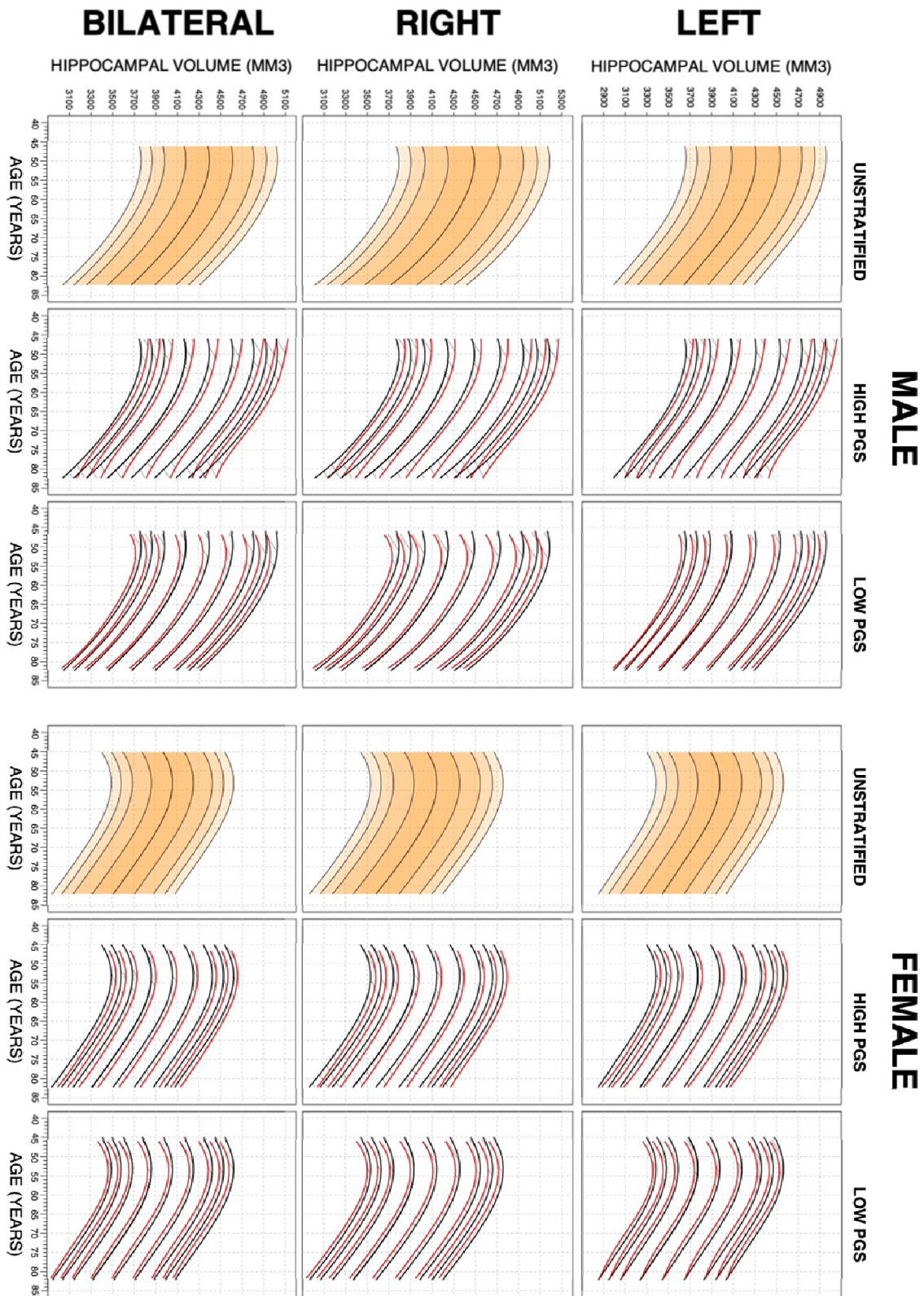


Figure 3 – Figure Supplement 2: Summary of PGSs and models based on HV GWAS and ADNI samples. The left set of graphs show the R-Squared of the regression models of PRS across HV for the scores built across SNP P-Value thresholds. In contrast to the graphs seen in the UKB samples, the R-squared values for the most part increase with p-value threshold. The set of graphs on the right show the spread of HV across PGS percentiles, each at the score that had the highest R-Squared value from the corresponding left graph.

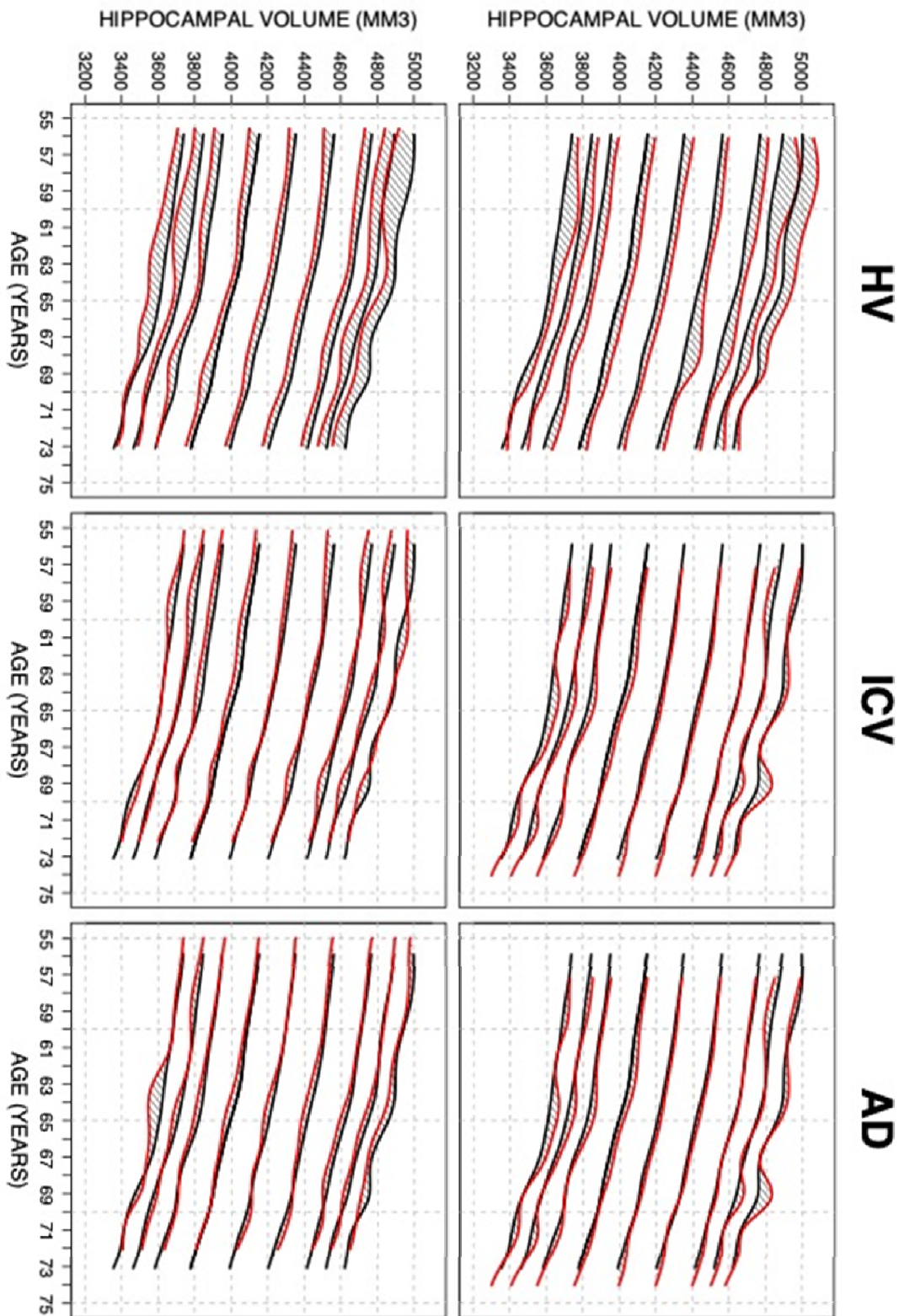
1082
 1083
 1084
 1085
 1086
 1087
 1088
 1089
 1090
 1091
 1092
 1093
 1094
 1095
 1096
 1097
 1098
 1099
 1100
 1101
 1102
 1103
 1104
 1105
 1106
 1107
 1108
 1109
 1110
 1111
 1112
 1113
 1114
 1115
 1116
 1117
 1118
 1119
 1120
 1121
 1122
 1123
 1124



1125 **Figure 4 – Figure Supplement 1: Genetically Adjusted Nomograms.** For all sub-figures, the
 1126 black lines -from top to bottom- represent the 2.5%, 5%, 10%, 25%, 50%, 75%, 90%, 95%,
 1127 and 97.5% quantiles respectively.

LOW PGS

HIGH PGS



1128
1129
1130
1131
1132
1133
1134
1135
1136
1137
1138
1139
1140
1141
1142
1143
1144
1145
1146
1147
1148
1149
1150
1151
1152
1153
1154
1155
1156
1157
1158
1159
1160
1161
1162
1163
1164
1165
1166
1167
1168

1169 **Figure 4 – Figure Supplement 2:** Nomograms generated with the SWM by stratifying the
1170 sample set based on PGSs. Left column: PGS based on HV GWAS. Middle column: PGS based
1171 on ICV GWAS. Right column: PGS based on AD GWAS. For all sub-figures, the black lines -
1172 from top to bottom-represent the 2.5%, 5%, 10%, 25%, 50%, 75%, 90%, 95%, and 97.5%
1173 quantiles respectively.

1174
1175
1176
1177
1178
1179
1180
1181
1182
1183
1184
1185
1186
1187
1188
1189
1190
1191
1192
1193
1194
1195
1196
1197
1198
1199
1200
1201
1202
1203
1204
1205
1206
1207
1208
1209
1210
1211
1212
1213
1214
1215
1216
1217
1218
1219
1220

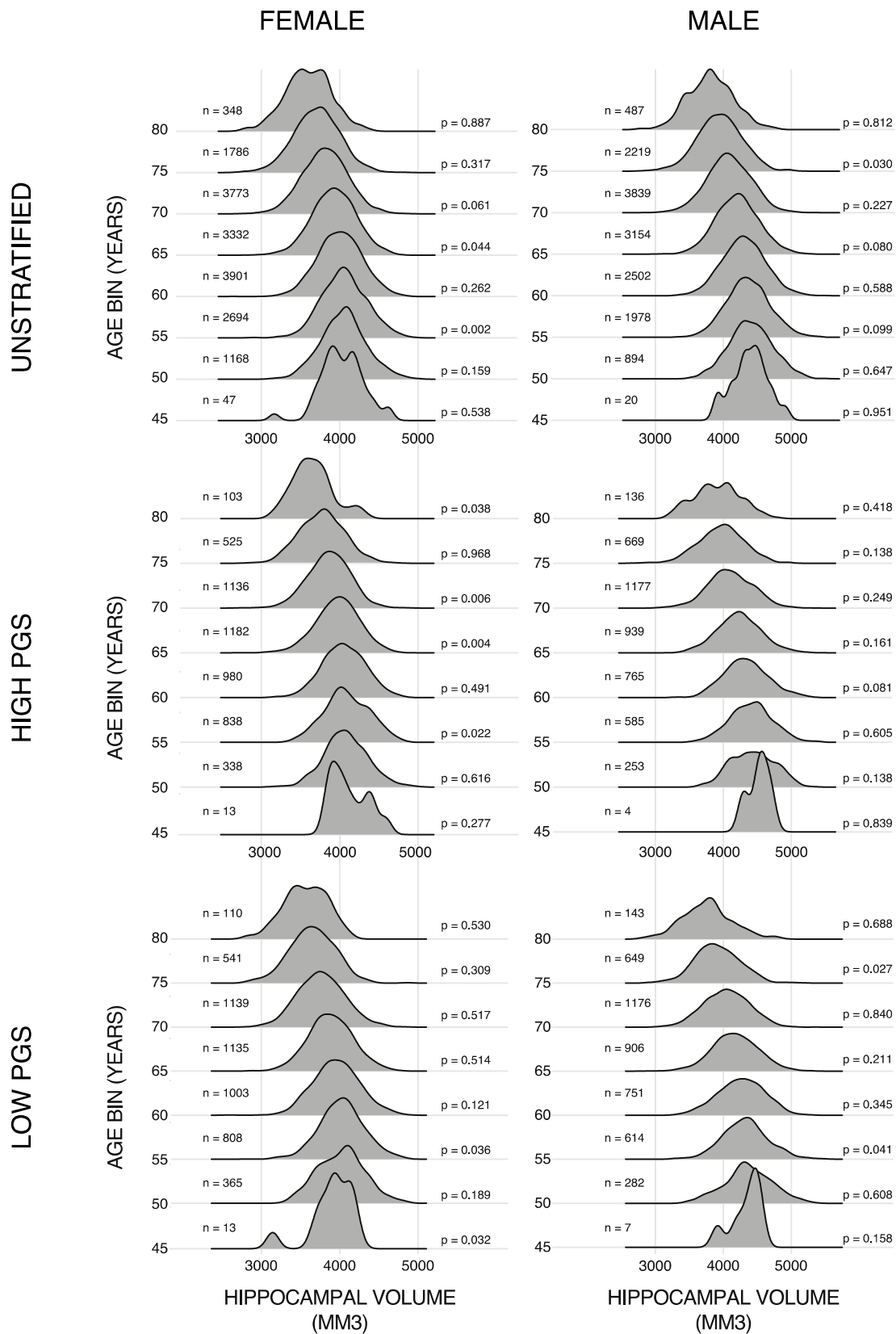


Figure 4 – Figure Supplement 3: Training Data Ridge Plots. Histograms of bilateral HV across the different subsets of the datasets. Samples are grouped in bins of 5 years. N is the number of samples in each set and p is the p-value from a Shapiro-Wilk (SW) test of normality. Typically, this test would indicate a non-gaussian distribution with a p-value lower than 0.05 (0.001 corrected for 48 multiple tests in this case).